UNIVERSITY OF CRETE

MASTER'S THESIS

Spin-polarized atoms and molecules in magnetic fields

Author:
Chrysovalantis KANNIS

Supervisor:
Prof. Peter RAKITZIS

A thesis submitted in partial fulfillment of the requirements for the Master's degree

in the

Department of Physics

October 19, 2017

UNIVERSITY OF CRETE

Abstract

Department of Physics

Spin-polarized atoms and molecules in magnetic fields

by Chrysovalantis KANNIS

The ability to control the spin of electrons and nuclei is of great importance to many scientific and technological fields, such as MRI (Magnetic Resonance Imaging) and the study of nuclear reactions. It is well known that completely polarizing the nuclear spins in the D-T and D-^{3}He reactions increases the fusion cross section by $\sim$50%; however, such effects have not yet been measured in a plasma, because of the lack of high-density spin polarized atoms. Recently, high-density spin-polarized atoms have been produced by molecular photodissociation, however the standard (optical) methods of detection cannot be used as the sample is too thick. Moreover, in both NMR-related applications and in the environment of a nuclear reactor, high magnetic fields are present. Therefore, it is crucial to study the interactions of spins in the presence of magnetic fields.

The first part of this thesis is dedicated to the theoretical study of depolarization of H, H_2, and HD in the presence of magnetic fields. In the second part we introduce a versatile method for measuring atomic polarization via the detection of macroscopic magnetization, which can be applied to high density samples (>10^{17} cm^{-3}) in contrast to optical methods, which are efficient only for lower density samples (<10^{13} cm^{-3}).

Acknowledgements

I would like to thank all the people who contributed in some way to the work described in this thesis. First and foremost, I thank my academic advisor, Professor T. Peter Rakitzis, for accepting me into his group. He contributed to a rewarding graduate school experience by engaging me in new ideas, and demanding a high quality of work in all my endeavors. Additionally, I would like to thank my committee members Professor Dimitris Charalambidis, and Dr. Wolf von Klitzing for their interest in my work.

Every result described in this thesis was accomplished with the help and support of fellow labmates and collaborators. Dr. Dimitris Sofikitis and I worked together on several different phases of this project, and without his efforts my job would have undoubtedly been more difficult. I greatly benefited from his keen scientific insight, his knack for solving seemingly intractable practical difficulties, and his ability to put complex ideas into simple terms. I would also like to thank Dr. George Katsoprinakis and Alexandros Spiliotis for the stimulating discussions.

Finally, I would like to acknowledge the Department of Physics and Foundation for Research and Technology. My graduate experience benefited greatly from the courses I took, the high-quality seminars that the department organized, and the experiments that I participated in.

Chrysovalantis Kannis

October 19, 2017

Contents

Chapter 1

Introduction

1.1 Applications of spin polarized atoms and molecules

The ability to prepare atomic and molecular samples in a non-thermal distribution of their electronic and nuclear spin, as well as the ability to characterize them, is of crucial importance in many fields. Various applications include the study of spin-dependent effects in atomic and nuclear collisions [1], the clarification of molecular structure and dynamics using NMR [2], and even schemes for quantum computation [3]. Methods for achieving such non-thermal, i.e. *polarized* distributions in atoms include Stern-Gerlach separation [4], optical pumping [5], and spin-exchange optical pumping [1], while, in some cases, polarized molecular ensembles have been prepared using spin-exchange optical pumping [6].

In addition, nuclear-spin-polarized atoms are useful for the study of nuclear reactions [7]. For example, the use of nuclear-spin-polarized reactants can increase or decrease the reaction cross sections, while also controlling the emission direction of products (with important benefits to the efficiency and the safety of reactors). Consequently, it is crucial to study the phenomenon of polarization in atoms and molecules, as a means of producing spin-polarized nuclei for nuclear fusion.

Nulcear spin-polarized molecules of hydrogen isotopes (e.g. H_2, HD, D_2, and DT) can be produced by cryogenic cooling in strong magnetic fields [8], Stern-Gerlach spin-separation [9], recombination of spin-polarized atoms at surfaces [10], and by rotational polarization through optical pumping followed by hyperfine beating (which transfers the rotational polarization to the nuclear spin) [11]. In the gas phase, the rotational polarization can be lost through collisions with other molecules or with the gas-cell walls; subsequently, the loss of rotational polarization produces a loss in nuclear polarization (also through the hyperfine beating mechanism). However, an external magnetic field can reduce the polarization transfer from the nuclear spin to the molecular rotation. In chapter 2 of this thesis, we present calculations for hyperfine beating in H, H_2, and HD, as a function of magnetic field. In this way, the B-field-dependent nuclear depolarization can be calculated, which is important for understanding and protecting spin-polarized molecules of hydrogen isotopes in magnetic fields.

Additionally, methods for measurement of polarized atoms, in high density, have not been developed. Conventional methods of measurement include optical measurements and atomic polarimeters; neither can be used here, as the density is too high (making the sample optically thick, and also not allowing an atomic beam for measurement in an atomic polarimeter). Recently, the Milner group has produced highly spin-polarized oxygen molecules, from the optical centrifuging of O_2 molecules [12]; subsequently, the rapid change in magnetization of the O_2 sample

was measured with a pick-up coil. In chapter 3 of this thesis, we describe the adaptation of this method for the measurement of spin-polarized atoms from the photodissociation of diatomic molecules.

Chapter 2

Depolarization of H, H_2, and HD in the presence of magnetic fields

2.1 Polarization transfer from molecular rotation to nuclear spin and vice versa

In general, molecules and atoms contain more than one angular momentum entities. These can be associated with molecular rotation, often symbolized as J, the electronic angular momentum L and intrinsic angular momentum (called spin) S and finally the nuclear spin I. The angular momentum entities associated with the electron are usually weakly coupled to the ones associated to the nuclei via the hyperfine interaction, thus they are considered to be independent from each other over relatively short timescales. The spins that have a random spatial distribution initially, couple to the molecular rotation J to produce a total angular momentum vector F. If the molecular rotation polarization is observed in subsequent times, it will be found to vary in an oscillating way. The oscillation is caused by the interaction of the electron and the nuclear spin. Consequently, this interaction leads to polarization exchange between the two of them. If we start with an ensemble of atoms with their electron spin totally oriented (e.g. $\Uparrow$) but with the nuclear spin unpolarized (i.e. $\uparrow, \downarrow$), then the half of the atomic population will go to one of the co-oriented, time-independent spin states ($|\Uparrow, \uparrow\rangle$) and the other half to one of the two counter-oriented, time-dependent spin states ($|\Uparrow, \downarrow\rangle, |\Downarrow, \uparrow\rangle$). Changing from one counter-oriented to the other spin states, causes the total polarization to bounce from the electronic to the nuclear spin on the sub-nanosecond timescale. Additionally, the molecular rotation is similarly coupled to the nuclear spin and polarization is transferred from the molecular rotation to the nuclear spin and back, but on much longer timescales (on the order of μs). Thus, photodissociation of the molecule at the appropriate time, when the nuclear spin is sufficiently polarized, can lead to the production of atoms with their nuclear spin polarized.

Various spin-physics experiments in high energy and nuclear physics use as targets polarized hydrogen and deuterium gases, such as the experiments performed by the HERMES Collaboration, which have studied, e.g. deep inelastic scattering of 27.6 GeV electrons from a polarized H target at DESY [13], while the polarization of atomic hydrogen can be monitored using atomic polarimeters. However, in such experiments, an important part of the population of the H atoms recombines into molecules, and it is not clear if the polarization is in this case conserved.

In their 2001 letter [14], T. Wise and co-workers try to shed light in this open question, while the same problem is examined by the Ralf W. Engels group in Forschungszentrum Jülich Institute for Nuclear Physics. For such a task to be achieved, we need to be able to model the polarization transfer between the molecular rotation and the

nuclear spins in the presence of magnetic fields. R. Altkorn et al. [15] developed a general expression for the rotational depolarization, using the "angular momentum algebra" (a brief description is given in section 2.3). Subsequently, P. Rakitzis extrapolated this method to develop the respective expression for the nuclear spin depolarization in the hierarchical approximation [16] and a year later L. Rubio-Lago et al. [17] developed the full solution, i.e. in the nonhierarchical coupling formalism. We need to mention that these solutions are reliable only for zero magnetic field, because they use the $|J, I, F, m_F\rangle$ basis, which is diagonal only if $B = 0$. So, in this chapter we develop a purely quantum mechanical method to study the depolarization of atoms and molecules in the presence of magnetic fields. Our results agree with the "angular momentum algebra" results (for $B = 0$), and in some cases (HD molecule) with the available experimental data [18].

2.2 Atomic Hydrogen in homogeneous magnetic field

The simplest case in which we can study polarization transfer between the electronic and the nuclear spin, and how this is affected is atomic hydrogen. For the cases examined in this thesis, the polarization is initially acquired by the electron and it is then transferred to the nuclear spin via the hyperfine interaction between the nucleus and the electron. However, the dynamics of this interaction, as well as the magnitude of the polarization which can be transferred can be severely modified by the presence of magnetic fields. In the first part of this thesis we will study how the polarization transfer is modified by the presence of magnetic fields, for atomic hydrogen, and the H_2 and HD molecules.

The hamiltonian [e.g. 19, chapter 6] which describes the interaction of a hydrogen atom with an external magnetic field $\vec{B}$ is:

$$H = -\vec{\mu}_{atom} \cdot \vec{B} + A\vec{I} \cdot \vec{J}, \tag{2.1}$$

where $\vec{\mu}_{atom}$ is the total atomic magnetic moment, A the hyperfine-structure constant, and $\vec{I}$, $\vec{J}$ are the nuclear and electronic angular momenta respectively. The total atomic magnetic moment of the atom is the sum of the electronic and nuclear moments, i.e. $\vec{\mu}_{atom} = -g_J\mu_B\vec{J} + g_I\mu_N\vec{I} \simeq -g_J\mu_B\vec{J}, \quad (\hbar = 1)$. Since $\mu_N \ll \mu_B$ we can neglect the nuclear contribution (for all but the most precise measurements), so that the hamiltonian for the interaction with an external field $\vec{B}$ is: $H = g_J\vec{\mu}_B \cdot \vec{B} + A\vec{I} \cdot \vec{J}$, defining the direction of $\vec{B}$ to be z-axis, we get $H = g_J\mu_B B J_z + A\vec{I} \cdot \vec{J}$. Employing $J_\pm = J_x \pm iJ_y$ and $I_\pm = I_x \pm iI_y$ into $\vec{I} \cdot \vec{J} = I_xJ_x + I_yJ_y + I_zJ_z$, the hamiltonian can be written as

$$H = g_J\mu_B B J_z + AI_zJ_z + \frac{1}{2}A(I_+J_- + I_-J_+). \tag{2.2}$$

Suppose that $J = \frac{1}{2}$ and $I = \frac{1}{2}$, yielding to the hamiltonian matrix in $|m_J, m_I\rangle$ representation:

$$H = \begin{bmatrix} \frac{1}{2}g_J\mu_B B + \frac{1}{4}A & 0 & 0 & 0 \\ 0 & \frac{1}{2}g_J\mu_B B - \frac{1}{4}A & \frac{1}{2}A & 0 \\ 0 & \frac{1}{2}A & -\frac{1}{2}g_J\mu_B B - \frac{1}{4}A & 0 \\ 0 & 0 & 0 & -\frac{1}{2}g_J\mu_B B + \frac{1}{4}A \end{bmatrix}.$$

In order to describe the time evolution of our system we need to solve the Schrödinger equation. Thus, we firstly diagonalize the matrix and calculate the eigenvectors and eigenvalues.

$$|1\rangle = |\Uparrow,\uparrow\rangle \qquad E_1 = \frac{1}{2}g_J\mu_B B + \frac{1}{4}A \tag{2.3}$$

$$|2\rangle = cos\theta\,|\Uparrow,\downarrow\rangle + sin\theta\,|\Downarrow,\uparrow\rangle \qquad E_2 = -\frac{1}{4}A + \frac{1}{2}g_J\mu_B B\sqrt{1+\left(\frac{A}{g_J\mu_B B}\right)^2} \tag{2.4}$$

$$|3\rangle = cos\theta\,|\Downarrow,\uparrow\rangle - sin\theta\,|\Uparrow,\downarrow\rangle \qquad E_3 = -\frac{1}{4}A - \frac{1}{2}g_J\mu_B B\sqrt{1+\left(\frac{A}{g_J\mu_B B}\right)^2} \tag{2.5}$$

$$|4\rangle = |\Downarrow,\downarrow\rangle \qquad E_4 = -\frac{1}{2}g_J\mu_B B + \frac{1}{4}A \tag{2.6}$$

where $tan2\theta = \frac{A}{g_J\mu_B B} = \frac{B_c}{B}$, $\quad B_c = \frac{A}{g_J\mu_B}$.
Figure (2.1) shows the energy of the four states as a function of the external magnetic field.

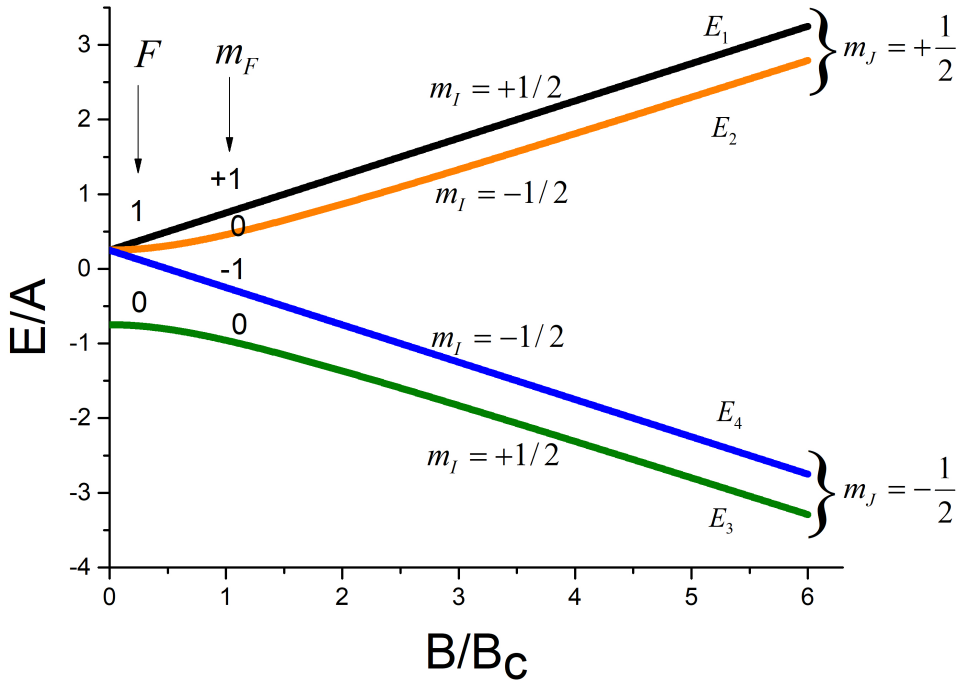

FIGURE 2.1: The energy of the four states as a function of the external magnetic field B.

Using the above equations we can write the hyperfine states with respect to the four eigenstates and evolve them in time, multiplying by the time evolution operator. In the following formulas $\hbar = 1$.

$$|\Uparrow,\uparrow\rangle_0 = |1\rangle \qquad |\Uparrow,\uparrow\rangle_t = e^{-iE_1 t}\,|1\rangle \tag{2.7}$$

$$|\Uparrow,\downarrow\rangle_0 = cos\theta\,|2\rangle - sin\theta\,|3\rangle \qquad |\Uparrow,\downarrow\rangle_t = e^{-iE_2 t}cos\theta\,|2\rangle - e^{-iE_3 t}sin\theta\,|3\rangle \tag{2.8}$$

$$|\Downarrow,\uparrow\rangle_0 = sin\theta\,|2\rangle + cos\theta\,|3\rangle \qquad |\Downarrow,\uparrow\rangle_t = e^{-iE_2 t}sin\theta\,|2\rangle + e^{-iE_3 t}cos\theta\,|3\rangle \tag{2.9}$$

$$|\Downarrow,\downarrow\rangle_0 = |4\rangle \qquad |\Downarrow,\downarrow\rangle_t = e^{-iE_4 t}\,|4\rangle \tag{2.10}$$

Now, we need to restore the units in order to determine the timescale for the beatings

of angular momenta projections. The critical field B_c for the atom of hydrogen is $B_c = 50.7\ mT$ [7], $\hbar = 1.0545718 \times 10^{-34} Js$, $\mu_B = 9.274 \times 10^{-24} J/T$. Suppose the atom is prepared with $m_J = +\frac{1}{2}$. The value of $\langle m \rangle$ is defined as

$$\langle m_{electron} \rangle = \frac{\sum_{m_I, m_J, m_{I'} = -1/2}^{1/2} m_J |\, {}_0\langle \Uparrow, m_I | m_J, m_{I'} \rangle_t \,|^2}{\sum_{m_I, m_J, m_{I'} = -1/2}^{1/2} |\, {}_0\langle \Uparrow, m_I | m_J, m_{I'} \rangle_t \,|^2} \tag{2.11}$$

for the electron and

$$\langle m_{proton} \rangle = \frac{\sum_{m_I, m_J, m_{I'} = -1/2}^{1/2} m_{I'} |\, {}_0\langle \Uparrow, m_I | m_J, m_{I'} \rangle_t \,|^2}{\sum_{m_I, m_J, m_{I'} = -1/2}^{1/2} |\, {}_0\langle \Uparrow, m_I | m_J, m_{I'} \rangle_t \,|^2} \tag{2.12}$$

for the proton. The respective graphs for different values of magnetic field are shown below. As figure (2.2) shows (for zero magnetic field), it is easy to notice that one

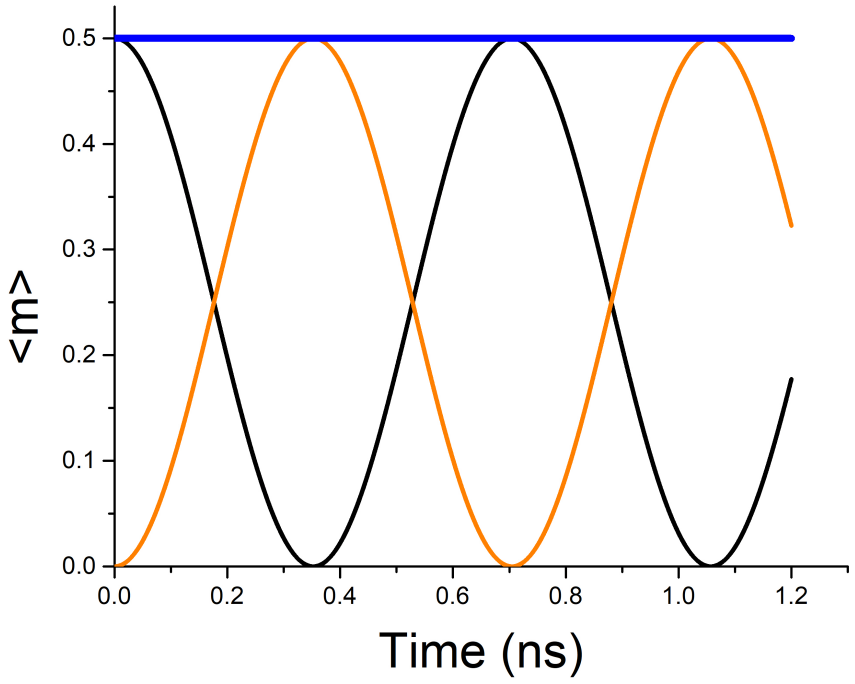

FIGURE 2.2: The value of the projection of J (black line), I (orange line), and their sum (blue line) for zero magnetic field.

period for $\langle m_{electron} \rangle$ (and for $\langle m_{proton} \rangle$) has a duration of $\sim 7 \times 10^{-10}$ s, i.e. $\lambda = c \cdot T \sim 21$ cm (that is microwave radio region)! This is the well-known hydrogen line, which is observed frequently in radio astronomy, since those radio waves can penetrate the large clouds of interstellar cosmic dust that are opaque to visible light. Thus, it is obvious that 21-cm line comes from the spin-flip transition of hydrogen. The other two figures (2.3,2.4) display the behavior of $\langle m_{electron} \rangle$, $\langle m_{proton} \rangle$ as the magnetic field increases. We infer that for large magnetic fields (large, comparing to B_c) the $\langle m_{electron} \rangle$ tends to $\frac{1}{2}$ and $\langle m_{proton} \rangle$ tends to 0. This is happening because the system was initially prepared at $m_J = +\frac{1}{2}$ states.

In addition, integrating the quantities $\langle m_{electron} \rangle$, and $\langle m_{proton} \rangle$ for a large amount

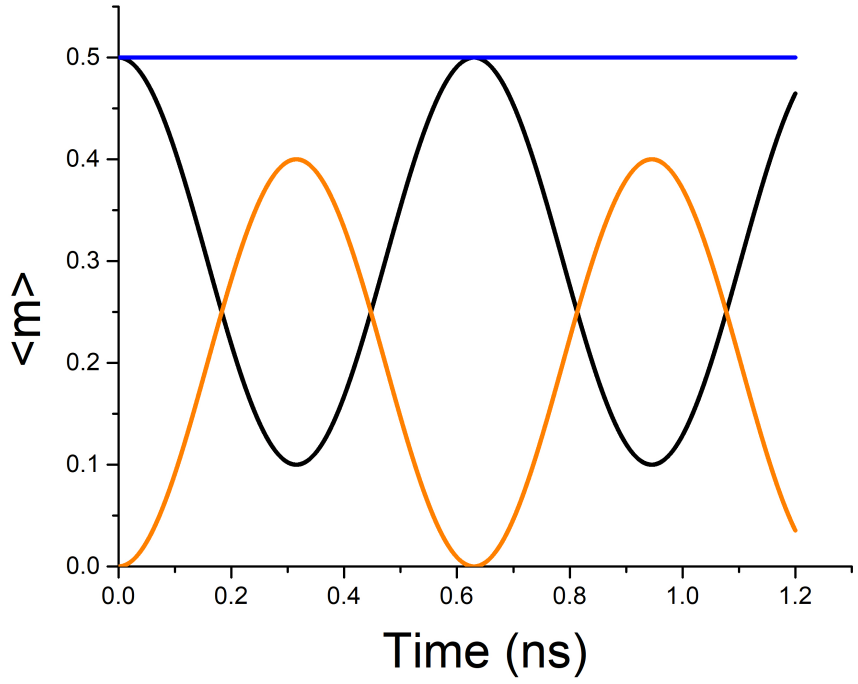

FIGURE 2.3: The value of the projection of J (black line), I (orange line), and their sum (blue line), for $B = 0.5B_c$.

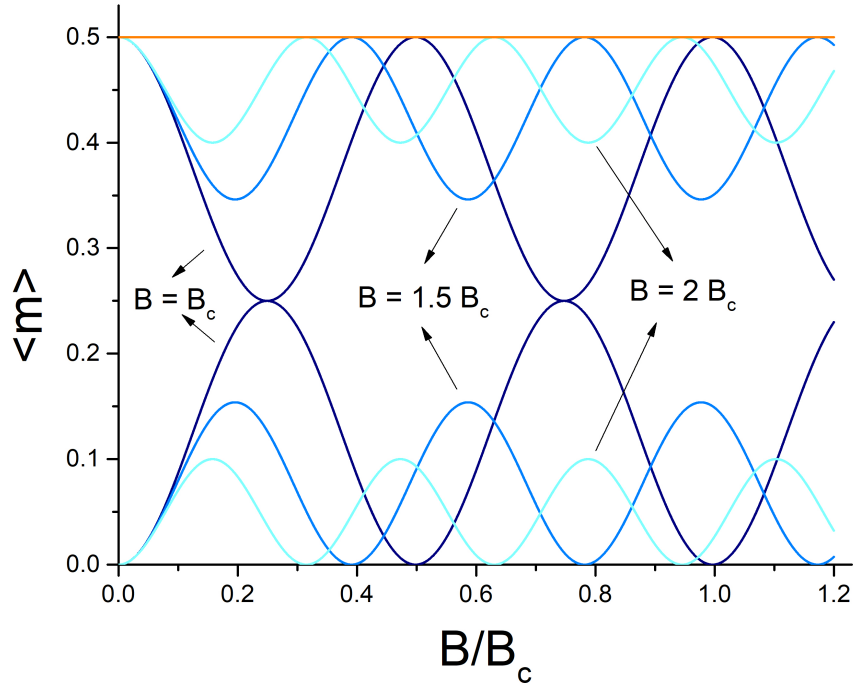

FIGURE 2.4: The value of the projection of J, I, and their sum, for $B = B_c, 1.5B_c, 2B_c$.

of time, that is $\langle m \rangle_{avg} = \lim_{T\to\infty} \frac{1}{T} \int_0^T \langle m \rangle \, dt$, one can obtain their behavior with respect to the external magnetic field. As it shown in figure (2.5) for large B the nuclear and rotational angular momenta do not interact with each other.

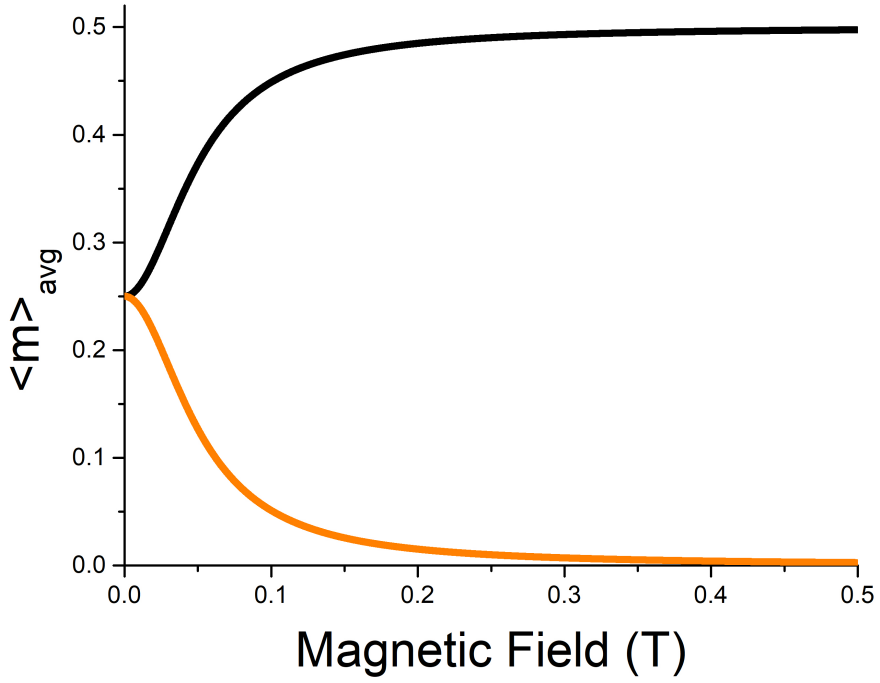

FIGURE 2.5: Graph of $\langle m \rangle_{avg}$ for the proton spin $I = \frac{1}{2}$ (orange line) and the electron spin $J = \frac{1}{2}$ (black line) with respect to magnetic field B.

2.3 H_2 molecule in external magnetic field

Norman F. Ramsey [20, 21] showed that the hamiltonian for a homonuclear diatomic molecule* in a magnetic field $\vec{B}$ is:

$$\begin{aligned} H/h = &-(1-\sigma_i(\vec{J}))a\vec{I}\cdot\frac{\vec{B}}{B} - (1-\sigma_J(\vec{J}))b\vec{J}\cdot\frac{\vec{B}}{B} - c\vec{I}\cdot\vec{J} \\ &+ \frac{5d}{(2J-1)(2J+3)}\left[3(\vec{I}\cdot\vec{J})^2 + \frac{3}{2}\vec{I}\cdot\vec{J} - \vec{I}^2\vec{J}^2\right] \\ &- \frac{5f}{3(2J-1)(2J+3)}\left[3\frac{(\vec{J}\cdot\vec{B})^2}{B^2} - \vec{J}^2\right] - g \end{aligned} \tag{2.13}$$

where $\vec{I}$ is the resultant spin angular momentum in units of $\hbar$ and $\vec{J}$ is the molecular rotational angular momentum also in $\hbar$ units. The first term in (2.13) corresponds to the interaction of the nuclear magnetic moments with the external magnetic fields and a is defined by

$$a = \frac{\mu_i B}{ih} \tag{2.14}$$

*except for $I = 1$ and $J = 2$

where μ_i is the magnetic moment of one of the nuclei and i the corresponding nuclear spin. The factor $(1 - \sigma_i(\vec{J}))$ arises from the magnetic shielding of the nucleus by the molecule. The second term in (2.13) includes the interaction of the molecular rotational magnetic moment with the external magnetic field field and b is defined by

$$b = \frac{\mu_J B}{Jh} \tag{2.15}$$

where μ_J is the magnetic moment due to the rotation of the molecule in the rotational state J. The third term corresponds to the spin rotational magnetic interaction. The fourth term provides for the combination of the spin-spin magnetic interaction of the two nuclei with each other together with the interaction of any nuclear electrical quadrupole moment with the variation of the molecular electric field in the vicinity of the nucleus. The last two terms in (2.13) are for the diamagnetic interaction of the molecule with the external magnetic field.
The case of greatest experimental interest is molecular hydrogen in the first rotational state of which $I = J = 1$. In this case, the magnetic shielding which arises in the spin-spin magnetic interaction should also be included, but this correction is negligibly small (of order 3×10^{-5}), as proved experimentally [22]. The diamagnetic constants [23] are too small as well, so these terms will be omitted in the following analysis. The values of the rest constants of the hamiltonian are shown in the table below:

Constant	H_2
a	$4.258 \times 10^4 B$
b	$0.6717 \times 10^4 B$
c	113.8
d	57.68

TABLE 2.1: The values for the constants in the hamiltonian. The constants are given in kHz and B in Tesla.[20]

Now, we are ready to calculate the hamiltonian matrix and diagonalize it. The eigenvalues of the hamiltonian correspond to the eigenenergies of H_2 which are plotted as functions of magnetic field B (figures 2.6,2.7). According to Abel–Ruffini theorem [24], there is no algebraic solution (i.e. solution in radicals) to the general polynomial equations of degree five or higher with arbitrary coefficients. In our system the characteristic polynomial is of order nine, and so the evaluation of eigenvalues and eigenvectors is achieved arithmetically (using Mathematica) and they cannot be written in close form (with radicals). The same procedure also applied to HD, where the hamiltonian is an 18×18 matrix.
As it is indicated (better) in figure (2.7) at zero magnetic field that we can distinguish the states in a quintuplet, a triplet and a singlet with energies $-84.96\ kHz$, $-30.4\ kHz$, and $516\ kHz$, respectively.

Suppose that the H_2 molecules are prepared ($t = 0$) in the state $m_J = +1$. The projection of nuclear and rotational angular momentum as a function of time is evaluated by the formulas:

$$\langle m_{nucl} \rangle = \frac{\sum_{m_I, m_J, m_{I'}=-1}^{1} m_{I'} |\, {}_0\langle +1, m_I | m_J, m_{I'} \rangle_t\, |^2}{\sum_{m_I, m_J, m_{I'}=-1}^{1} |\, {}_0\langle +1, m_I | m_J, m_{I'} \rangle_t\, |^2} \tag{2.16}$$

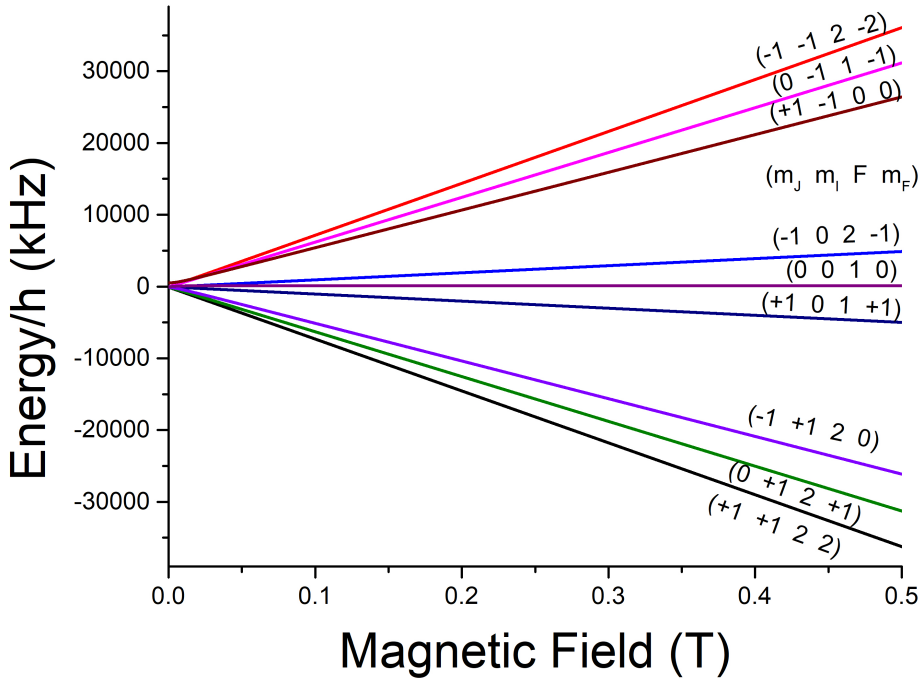

FIGURE 2.6: Energies of H_2 as functions of magnetic field B from 0 to 0.5 T.

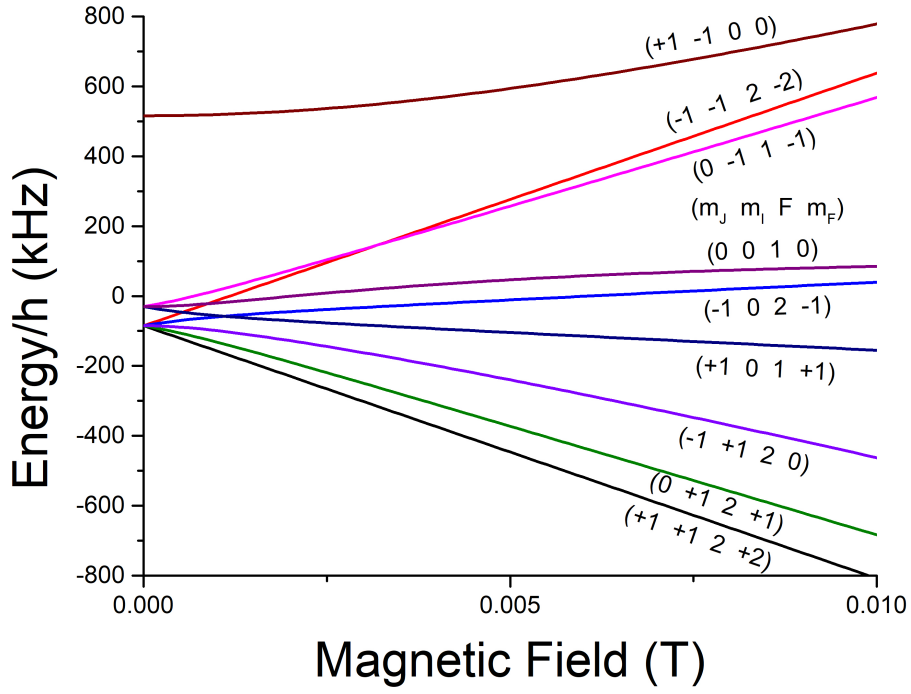

FIGURE 2.7: A zoom in. Energies of H_2 as functions of magnetic field B from 0 to 0.01 T.

and

$$\langle m_{rot} \rangle = \frac{\sum_{m_I,m_J,m_{I'}=-1}^{1} m_J |\, {}_0\langle +1, m_I | m_J, m_{I'} \rangle_t\,|^2}{\sum_{m_I,m_J,m_{I'}=-1}^{1} |\, {}_0\langle +1, m_I | m_J, m_{I'} \rangle_t\,|^2} \tag{2.17}$$

Applying the equations (2.16), and (2.17) for $B = 0$ we get the following figure (2.8). These results agree with the "angular momentum algebra" solution [15, 16], which is

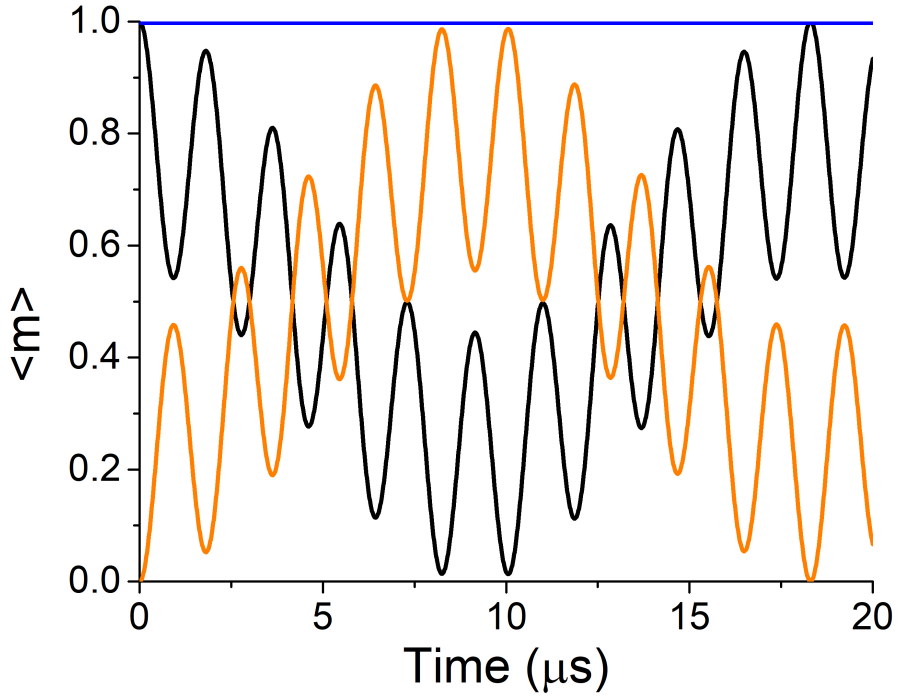

FIGURE 2.8: Time dependence of $\langle m \rangle$ for the nuclear spin $I = 1$ (orange line) and the rotational angular momentum $J = 1$ (black line). The sum of these two (blue line) is constant, and equal to one.

valid only for zero magnetic fields. A brief description of the method is given below:

Consider an ensemble of molecules, each with angular momentum J. The spatial distribution of their angular momenta may be described by the $(2J+1)^2$ density matrix elements $\rho_{m'm}$, or, equivalently, by the $(2J+1)^2$ multipole moments $A_q^{(k)}(J)$, with $k \leq 2J$. These two sets of parameters are related by the following expression [25]:

$$\rho_{m'm} = \sum_{k,q} \frac{(2k+1)[J(J+1)]^{k/2}}{c(k)\,\langle J||\, J^{(k)}\, ||J\rangle} (-1)^{I+q-m'} \begin{pmatrix} J & k & J \\ -m & q & m' \end{pmatrix} A_q^{(k)}(J). \tag{2.18}$$

Note that the diagonal elements $\rho_{m'm}$ of the density matrix describe the m-state populations, $p(J,m)$, of the ensemble. In the case that J couples with I via the hyperfine interaction, they give total angular momentum states described by the quantum number F, each having an associated hyperfine energy E_F. Coherent excitation of all of the hyperfine F states, and the subsequent time evolution of their wave functions, produces a time-dependent quantum beating of the $A_q^{(k)}(J,t)$, which has been

shown to be described by the depolarization factor $G^{(k)}(J,t)$:

$$A_q^{(k)}(J,t) = G^{(k)}(J,t)A_q^{(k)}(J,0) \tag{2.19}$$

where

$$G^{(k)}(J,t) = \sum_{F,F'} \frac{(2F'+1)(2F+1)}{2I+1} \begin{Bmatrix} F' & F & k \\ J & J & I \end{Bmatrix}^2 cos\Big(\frac{(E_F - E_{F'})t}{\hbar}\Big). \tag{2.20}$$

Using a similar derivation, it is possible to show that the spatial distribution of the nuclear spin I may be described by parameters $A_q^{(k)}(I,t)$, which may be related back to the original molecular polarization of J, $A_q^{(k)}(J,0)$, and a time-dependent polarization factor $H^{(k)}(I,t)$:

$$A_q^{(k)}(I,t) = H^{(k)}(I,t)A_q^{(k)}(J,0), \tag{2.21}$$

which is more complicated than the $G^{(k)}(J,t)$. For the complete form of $H^{(k)}(I,t)$ you can see reference [16].

Furthermore, integrating the quantities $\langle m_{nucl}\rangle$, and $\langle m_{rot}\rangle$ for a large amount of time, that is $\langle m\rangle_{avg} = \lim_{T\to\infty} \frac{1}{T}\int_0^T \langle m\rangle\, dt$, one can obtain their behavior with respect to the external magnetic field. As it shown in figure (2.9) for large B the nuclear and rotational angular momenta do not interact with each other.

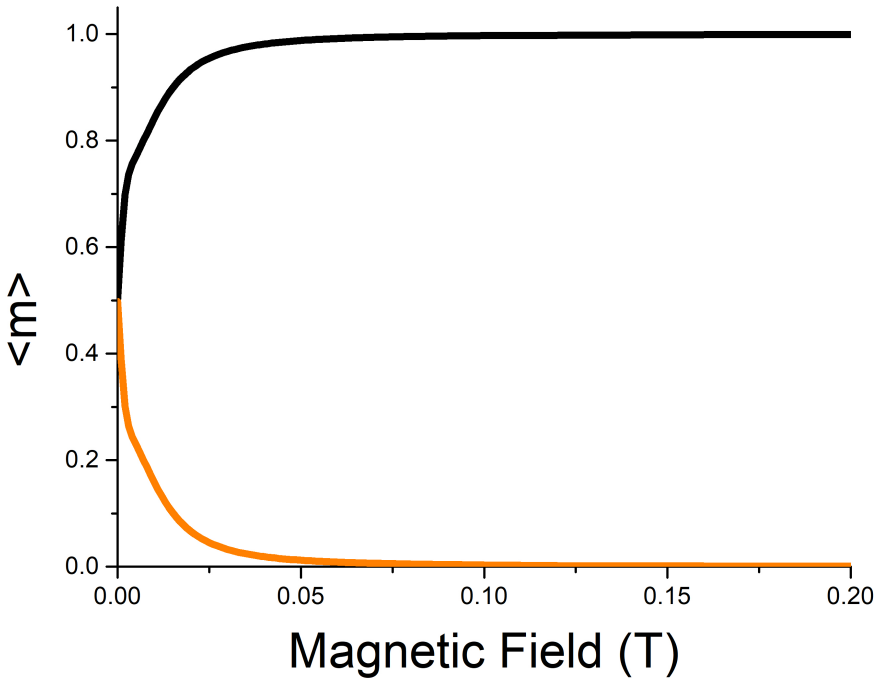

FIGURE 2.9: Graph of $\langle m\rangle_{avg}$ for the nuclear spin $I = 1$ (orange line) and the rotational angular momentum $J = 1$ (black line) with respect to magnetic field B.

2.4 HD molecule in external magnetic field

Eventually, after studying these two simple cases, we can apply the same procedure for a more complicated molecule, HD. The only difference is that now instead of two different angular momenta, we have three, because the nuclear spins (for H and D) are not equal.

Norman F. Ramsey and Henry R. Lewis, in their paper "Theory of Hydrogen Deuteride in Magnetic Fields" (see [26, 27]), define the hamiltonian for HD molecule as:

$$\begin{aligned} H/h = &-(1-\sigma_p(\vec{J}))a_p\vec{i}_p\cdot\frac{\vec{B}}{B}-(1-\sigma_d(\vec{J}))a_d\vec{i}_d\cdot\frac{\vec{B}}{B} \\ &-(1-\sigma_J(\vec{J}))b\vec{J}\cdot\frac{\vec{B}}{B}-c_p\vec{i}_p\cdot\vec{J}-c_d\vec{i}_d\cdot\vec{J} \\ &+\frac{5d_1}{(2J-1)(2J+3)}\Big[\frac{3}{2}(\vec{i}_p\cdot\vec{J})(\vec{i}_d\cdot\vec{J})+\frac{3}{2}(\vec{i}_d\cdot\vec{J})(\vec{i}_p\cdot\vec{J})-\vec{i}_p\cdot\vec{i}_d\vec{J}^2\Big] \\ &+\frac{5d_2}{(2J-1)(2J+3)}\Big[3(\vec{i}_d\cdot\vec{J})^2+\frac{3}{2}(\vec{i}_d\cdot\vec{J})-\vec{i}_d^2\vec{J}^2\Big] \\ &-\frac{5f}{3(2J-1)(2J+3)}\Big[3\frac{(\vec{J}\cdot\vec{B})^2}{B^2}-\vec{J}^2\Big]-g+\delta\vec{i}_p\cdot\vec{i}_d \end{aligned} \tag{2.22}$$

where $\vec{i}_p$ and $\vec{i}_d$ are the spin angular momenta of the proton and deuteron, respectively, in units of $\hbar$ and $\vec{J}$ is the molecular rotational angular momentum.

The first two terms in (2.22) correspond to the interactions of the nuclear magnetic moments with the external magnetic fields and the a's of the proton and deuteron respectively are given by

$$a_p = \frac{2\mu_p B}{h}, \tag{2.23}$$

$$a_d = \frac{\mu_d B}{h}, \tag{2.24}$$

where μ_p and μ_d are proton and deuteron magnetic moments, and $\sigma_p(\vec{J})$, $\sigma_d(\vec{J})$, $\sigma_J(\vec{J})$ are the magnetic shielding constants.
The third term in equation (2.22) includes the interaction of the molecular rotational magnetic moment with the external magnetic field and b is defined by

$$b = \frac{\mu_J B}{Jh}, \tag{2.25}$$

where μ_J is the magnetic moment due to the rotation of the molecule in rotational state J. The fourth and fifth terms correspond to the spin rotational magnetic interaction. The sixth term provides for the direct spin-spin magnetic interaction between the two nuclei together with a small contribution from the tensor portion of the electron coupled nuclear spin-spin interaction. The seventh term represents the interaction of the electric quadrupole moment of the deuteron. The eighth term arises from the orientation dependence of the diamagnetic susceptibility. The ninth term includes the orientation independent molecular susceptibility and is of no significance in experiments for which all transitions involve only changes of orientation of $\vec{i}_p$, $\vec{i}_d$, or $\vec{J}$, [28]. The last term corresponds to the portion of the electron coupled nuclear spin-spin interaction that depends only on the nuclear orientation.

In the rotational state $J = 0$, all orientations of the HD molecule are equally probable as a result that the interactions of interest average to zero; the hamiltonian reduces to the first two and last terms. Therefore, the first rotational state $J = 1$ is the case of greatest experimental interest. In this case the values of the constants are given in the following table (2.2).

Constant	HD
$(1-\sigma_p(1))a_p$	$4257.796 \times 10^4 B$
$(1-\sigma_d(1))a_d$	$653.5832 \times 10^4 B$
$(1-\sigma_J(1))b$	$505.5870 \times 10^4 B$
c_p	85589
c_d	13118
d_1	17764
d_2	-22452
f	$-26.3 \times 10^2 B^2$
δ	43

TABLE 2.2: The values for the constants in the hamiltonian. The constants are given in Hz and B in Tesla.[26]

Substituting the above constants into the hamiltonian and diagonalizing it, one can plot the eigenenergies of HD as a function of the external magnetic field. The representation most appropriate to a very weak magnetic field is not trivial. With only two interacting vectors, a simple F, m_F representation is appropriate in very weak fields. However no such simple representation is available for three interacting vectors, as in HD. The nature of the coupling in zero-field limit for HD depends on the relative magnitudes of the $\vec{i}_p - \vec{i}_d$ interactions, the $\vec{J} - \vec{i}_p$ interactions, and the $\vec{J} - \vec{i}_d$ interactions. Nevertheless, in order to distinguish the states we can use the F, m_F, F_{int} representation, where

$$\vec{F} = \vec{J} + \vec{i}_p + \vec{i}_d \tag{2.26}$$

$$\vec{F}_{int} = \vec{J} + \vec{i}_d \tag{2.27}$$

For $J = 1$, $i_p = \frac{1}{2}$, $i_d = 1$, F_{int} becomes $F_{int} = 0, 1, 2$ and the respective (F, F_{int}) are

$$(F, F_{int}) = \begin{cases} \left(\frac{1}{2}, 0\right) \\ \left(\frac{1}{2}, 1\right), \quad \left(\frac{3}{2}, 1\right) \\ \left(\frac{3}{2}, 2\right), \quad \left(\frac{5}{2}, 2\right) \end{cases}$$

The following figures show the energy for both of eighteen states of HD. Figure (2.10) shows the energies for B from 0 to 1 T, and figure (2.11) indicates the corresponding F, m_F of states. The second figure also displays the degeneration of states for zero magnetic field.

Suppose that HD molecules are prepared ($t = 0$) in the state $m_J = +1$. The projections of nuclear and rotational angular momenta as a function of time are evaluated by the formulas:

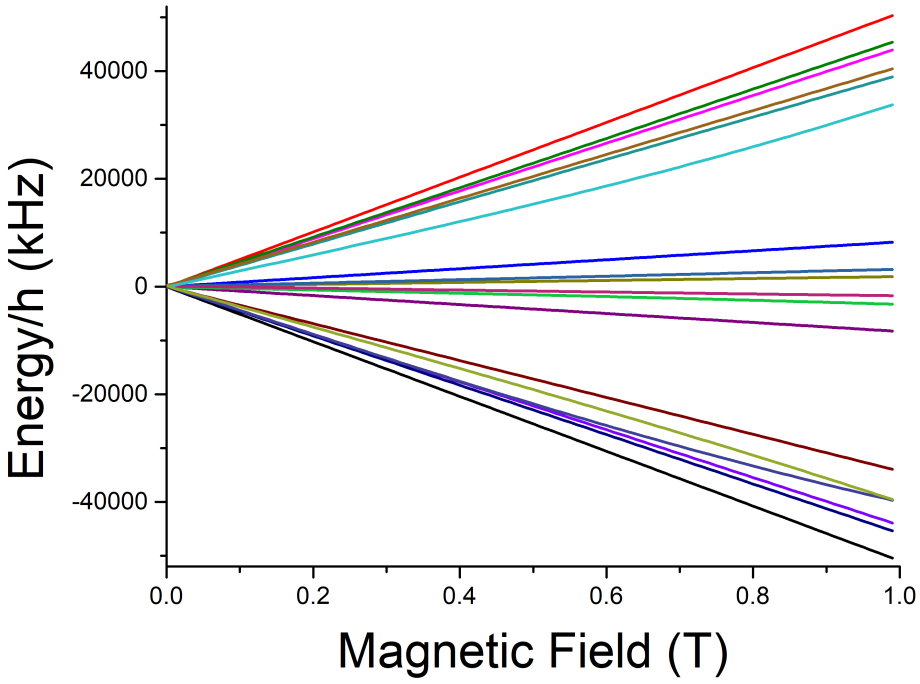

FIGURE 2.10: The energy of the eighteen states as a function of the external magnetic field B.

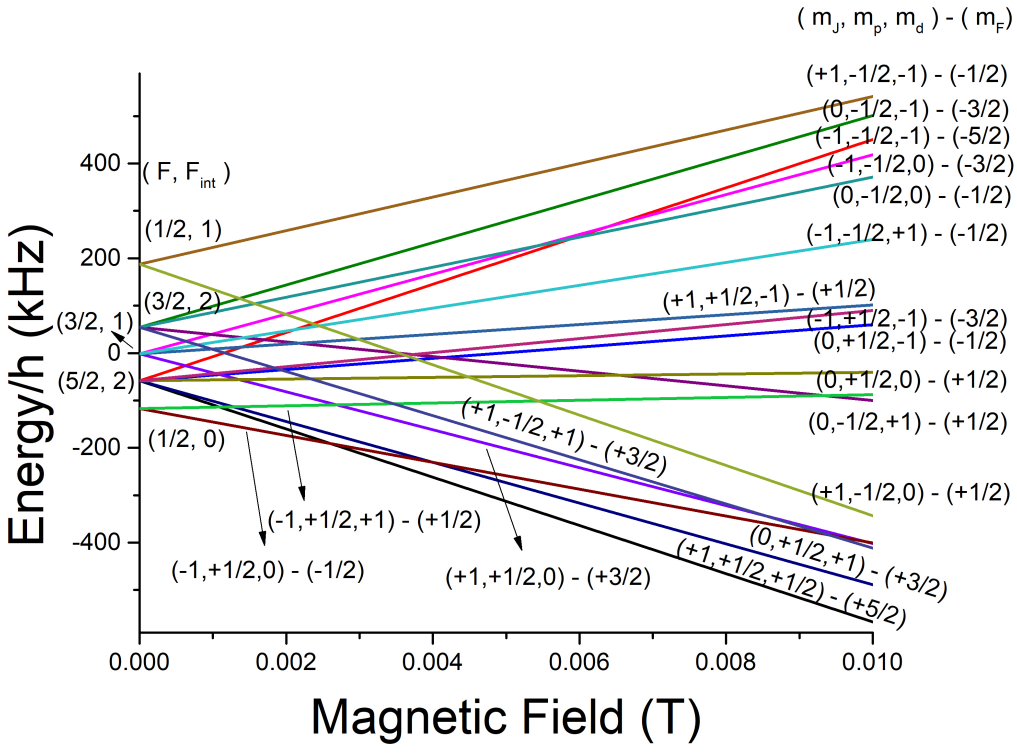

FIGURE 2.11: A zoom in. Energies of HD as functions of magnetic field B from 0 to 0.01 T.

$$\langle m_p \rangle = \frac{\sum_{m_{I_1},m_J,m_{I_1'}=1,m_{I_2},m_{I_2'}=1/2}^{m_{I_1},m_J,m_{I_1'}=1,m_{I_2},m_{I_2'}=1/2} m_{I_2'} |\, {}_0\langle +1, m_{I_1}, m_{I_2} | m_J, m_{I_1'}, m_{I_2'} \rangle_t\, |^2}{\sum_{m_{I_1},m_J,m_{I_1'}=-1,m_{I_2},m_{I_2'}=-1/2}^{m_{I_1},m_J,m_{I_1'}=1,m_{I_2},m_{I_2'}=1/2} |\, {}_0\langle +1, m_{I_1}, m_{I_2} | m_J, m_{I_1'}, m_{I_2'} \rangle_t\, |^2}, \tag{2.28}$$

$$\langle m_d \rangle = \frac{\sum_{m_{I_1},m_J,m_{I_1'}=1,m_{I_2},m_{I_2'}=1/2}^{m_{I_1},m_J,m_{I_1'}=1,m_{I_2},m_{I_2'}=1/2} m_{I_1'} |\, {}_0\langle +1, m_{I_1}, m_{I_2} | m_J, m_{I_1'}, m_{I_2'} \rangle_t\, |^2}{\sum_{m_{I_1},m_J,m_{I_1'}=-1,m_{I_2},m_{I_2'}=-1/2}^{m_{I_1},m_J,m_{I_1'}=1,m_{I_2},m_{I_2'}=1/2} |\, {}_0\langle +1, m_{I_1}, m_{I_2} | m_J, m_{I_1'}, m_{I_2'} \rangle_t\, |^2}, \tag{2.29}$$

$$\langle m_{rot} \rangle = \frac{\sum_{m_{I_1},m_J,m_{I_1'}=1,m_{I_2},m_{I_2'}=1/2}^{m_{I_1},m_J,m_{I_1'}=1,m_{I_2},m_{I_2'}=1/2} m_J |\, {}_0\langle +1, m_{I_1}, m_{I_2} | m_J, m_{I_1'}, m_{I_2'} \rangle_t\, |^2}{\sum_{m_{I_1},m_J,m_{I_1'}=-1,m_{I_2},m_{I_2'}=-1/2}^{m_{I_1},m_J,m_{I_1'}=1,m_{I_2},m_{I_2'}=1/2} |\, {}_0\langle +1, m_{I_1}, m_{I_2} | m_J, m_{I_1'}, m_{I_2'} \rangle_t\, |^2} \tag{2.30}$$

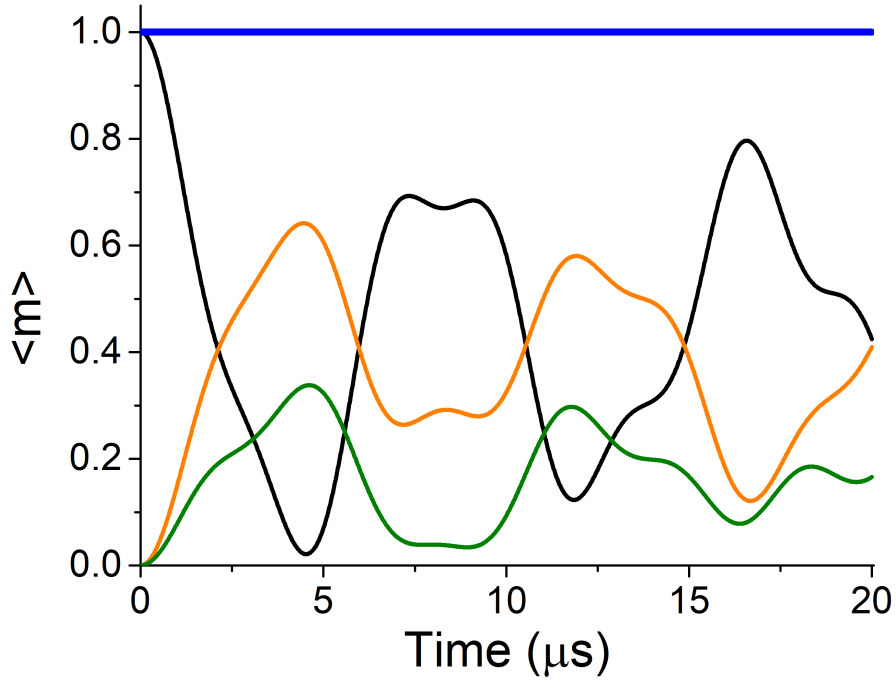

FIGURE 2.12: Time dependence of $\langle m \rangle$ for the deuterium nuclear spin $I_1 = 1$ (orange line), hydrogen nuclear spin $I_2 = \frac{1}{2}$ (green line) and the rotational angular momentum $J = 1$ (black line). Their sum is a constant equal to 1 (blue line).

Applying the equations (2.28), (2.29), and (2.30) for $B = 0$ we get the following figure (2.12). These results agree with both the "algebra momentum algebra" results [16] and the respective experimental data [18].

In addition, integrating the above quantities ($\langle m_p \rangle$, $\langle m_d \rangle$, $\langle m_{rot} \rangle$) for a large amount of time, i.e. $\langle m \rangle_{avg} = \lim_{T\to\infty} \frac{1}{T} \int_0^T \langle m \rangle \, dt$, one can obtain their behavior with respect to

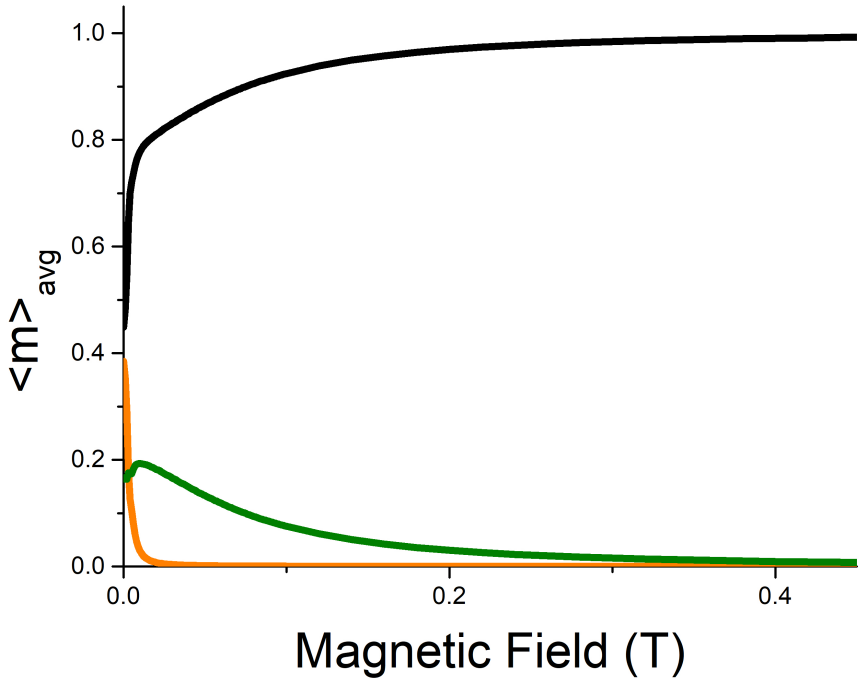

FIGURE 2.13: Graph of $\langle m \rangle_{avg}$ for the deuterium nuclear spin $I_1 = 1$ (orange line), hydrogen nuclear spin $I_2 = \frac{1}{2}$ (green line) and the rotational angular momentum $J = 1$ (black line) with respect to magnetic field B.

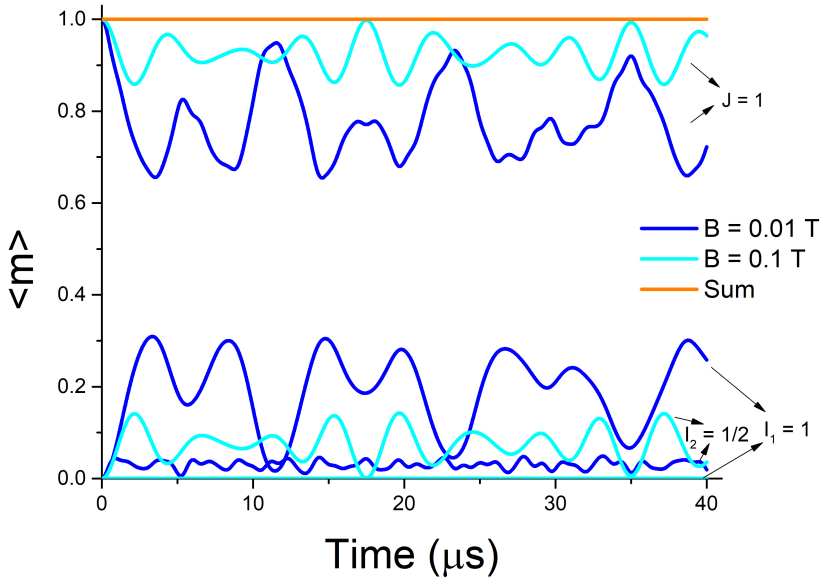

FIGURE 2.14: Graph of $\langle m \rangle$ for the deuterium nuclear spin $I_1 = 1$, hydrogen nuclear spin $I_2 = \frac{1}{2}$ and the rotational angular momentum $J = 1$ for $B = 0.1T$ and $B = 0.01T$.

the external magnetic field. As it shown in figure (2.13) for large B the nuclear and rotational angular momenta do not interact with each other. It is also noticeable that at very low fields, the D nucleus couples to the H nucleus, and can steal some polarization. However, at higher fields, the D nucleus is decoupled, and the H nucleus alone steals from J. Consequently, it is worth plotting the beatings for $B = 0.01\ T$ (maximum $\langle m \rangle$ for this magnetic field), and $B = 0.1\ T$ (figure 2.14).

HD is very similar to DT (same nuclear spins), and hence studying HD molecules allow us to draw general conclusions for DT as well. The study of depolarization dynamics of these molecules in the presence of magnetic fields offers important information for nuclear physics and other, polarization-related experiments. These results can be useful for experiments where molecules with either their rotational angular momentum or their nuclear spin is initially polarized. Since the polarization transfer is a function of the magnetic field, these graphs can be used in order to determine which magnetic fields are sufficient in order to prevent depolarization for a given timescale.

Chapter 3

Detection of macroscopic polarization

3.1 Methods for the production and detection of polarized atoms

In this chapter, we will focus on experimental methods for the production and detection of polarization in atoms and molecules, with emphasis on hydrogen and deuterium atoms.

We will begin by describing a laser-based method for the production of macroscopic polarized samples developed by the Polarization Spectroscopy group in IESL-FORTH. This method take advantage of the dissociation dynamics of small molecules to initially polarize the electronic spin of the atomic photo-fragments. A second method, which relies on the hyperfine depolarization beating to transfer this polarization to the nuclear spin, is described in the introduction of chapter 2.

In the following, we will describe the experimental methods used to detect this polarization in hydrogen and deuterium atoms. We will describe how this can be done either *indirectly* using 2+1 Resonance Enhanced Multi Photon Ionization (REMPI) [29], or *directly* using Laser Induced Fluorescence (LIF) [30].

Finally, we will describe a recently demonstrated method for the detection of atomic polarization through the detection of the macroscopic magnetization [12]. This is a versatile method that can be used for a variety of atoms and molecules, and most importantly, can be used in high-density samples, where most laser-based methods cannot. This method has been demonstrated recently by detecting the electronic polarization induced in O_2 molecules using an "optical centrifuge". The adaptation of this method to the detection of polarization induced in the atomic photofragments after molecular dissociation is the experimental part of this work. The final goal is to use this method to detect the polarization in high-density ($\sim 10^{18}$ cm^{-3}) deuterium atoms produced from the dissociation of Deuterium Iodide (DI). Such high-density polarized deuterium atoms can be combined with laser fusion to measure polarized D-D fusion cross sections [31]. However, we begin our experimental effort by detecting the polarization of chlorine atoms produced by dissociation of Cl_2 molecules, due to the availability of Cl_2 gas and the appropriate laser sources.

3.1.1 Preparation of polarized atoms from molecular photodissociation

In 1968 van Brunt and Zare first introduced the production of high-density polarized atoms by photodissociation of diatomic molecules [32]. This technique exploits the fact that the projection of the molecular electronic angular momentum, for prompt

photodissociation, is conserved within the atomic photofragments. In fact, the electronic states of diatomic molecules correlate adiabatically, at large internuclear separation, to atoms in specific $|JM\rangle$ states:

$$AB(\Omega_i) \longrightarrow A(J_A, M_A) + B(J_B, M_B) \tag{3.1}$$

where AB is a diatomic molecule, Ω_i is the projection of the total electronic angular momentum of electronic state i along the AB bond axis, and (J_A, M_A) and (J_B, M_B) are the atomic states of atoms A and B, respectively. Conservation of angular momentum projection along the recoil direction yields the constraint:

$$\Omega_i = M_A + M_B \tag{3.2}$$

For optical excitation of a particular Ω_i state, prompt adiabatic dissociation will produce atoms in particular M states.

As an example let us consider the prompt photodissociation of HCl molecules by circularly polarized light. The absorption of left circularly polarized light ($\sigma = -1$) (propagating parallel to the HCl bond) by ground state HCl ($\Omega = 0$) produces excited state HCl with $\Omega = -1$. In the dissociation step, the conservation of Ω the photofragment's angular momentum projections M_H and M_{Cl} produces polarized atoms (figure 3.1).

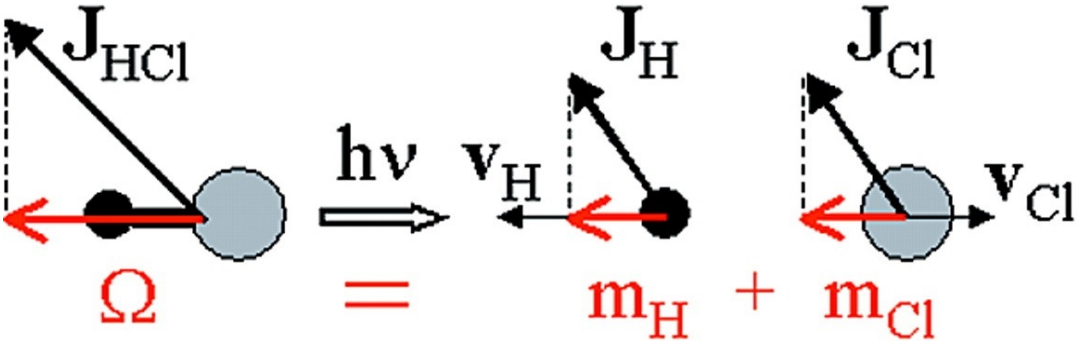

FIGURE 3.1: Photodisociation of excited HCl ($\Omega = -1$) with circularly polarized light (figure adapted from reference [33]).

3.2 Production and detection of spin polarized hydrogen (SPH) atoms

The technique for the production of polarized atoms through molecular photodissociation described in paragraph 3.1.1, although proposed in 1968 [32] it remained without significant experimental exploitation, especially due to the lack of intense laser sources. The development of pulsed lasers provided with the possibility to explore the production of polarized atoms this way, as well as their detection.

Hydrogen is the simplest and one of the most important atoms. However, the optical production or direct detection of spin-polarized hydrogen (SPH) atoms has proven to be very difficult. Polarized nuclei can be produced effectively by the Stern–Gerlach separation [4] and the polarization purity attainable using this technique can be as high as 100%. Nonetheless, the production rates are relatively low (about 10^{15} atoms per second) and the time resolution is poor. Another approach, which can yield high-density polarized nuclei, is optical pumping. Unfortunately,

optical pumping is not practical for hydrogen, as continuous-wave light sources with an energy corresponding to the 1s→2p transition (121.6 nm) are not commonly available.

3.2.1 Production of SPH from molecular photodissociation and indirect detection

In the initial experiments where it was shown that spin polarized hydrogen atoms can be prepared using molecular photodissociation, the polarization detection was done indirectly. The development of the direct detection method is described in the next paragraph (3.2.2). The problem of the hyperfine depolarization, which gave the initiative for the development of the technique of polarization transfer from the molecular rotation to the nuclear spin, became evident through the analysis of these experiments. Thus, it is natural to start by describing these experiments, both for practical and historical reasons.

The photodissociation of HCl at 193 nm satisfies the necessary requirements as a potential candidate for the production of state-selected photofragments: the optical excitation accesses predominantly (98%) a single excited state (the A $^1\Pi_1$ state via a perpendicular transition) with $|\Omega| = 1$, and yields photofragments with small angular momentum values. For molecules with their bonds lying exactly parallel to the photolysis laser propagation direction, excitation with right ($\sigma = +1$) or left ($\sigma = -1$) circularly polarized light selectively accesses the $\Omega = +1$ and $\Omega = -1$ excited states, respectively, which then dissociate, conserving the projection Ω as the sum of the atomic projections m_H and m_{Cl}. For molecules with bonds that are not parallel to the photolysis laser propagation direction (i.e. at an angle θ to this direction), the final polarization P of the fragments will be reduced by a factor of $cos\theta$ with respect to the polarization for $\theta = 0$ (assuming that there are negligible contributions from parallel transitions, which is true in this case). In addition, the average polarization of all photofragments (averaged over all angles for a pure perpendicular transition) is $P/2$. For dissociations, which involve a coherent excitation of both parallel and perpendicular transitions, a full quantum mechanical treatment [34], has been used.

The A $^1\Pi_1$ state with $\Omega = +1$ adiabatically correlates to "spin-down" H atoms with $m_H = -1/2$ (opposite sign to Ω). For $\Omega = -1$, all the signs are reversed:

$$HCl(A^1\Pi_1; \Omega = +1) \longrightarrow \quad H(m_H = -1/2) \quad + \quad Cl(m_{Cl} = +3/2) \tag{3.3}$$

However, the prompt dissociation may also proceed nonadiabatically, via a mechanism that involves an H atom spin flip. This occurs either through the a$^3\Pi_1$ state, which yields products in their electronic ground states, or through a second pathway, which leads to electronically (spin–orbit) excited Cl ($^2P_{1/2}$). Henceforth, the latter will also be referred as Cl^*.

$$HCl(\mathrm{a}^3\Pi_1; \Omega = +1) \longrightarrow \quad H(m_H = +1/2) \quad + \quad Cl(m_{Cl} = +1/2) \tag{3.4}$$

$$HCl(\Omega = +1) \longrightarrow \quad H(m_H = +1/2) \quad + \quad Cl^*(m_{Cl^*} = +1/2) \tag{3.5}$$

If either the spin-down channel (equation 3.3) or the spin-up channel (equations 3.4, 3.5) dominates, then spin polarized hydrogen (SPH) will be produced. The degree of nascent SPH produced by the photodissociation must be probed before secondary collisions can cause relaxation, preferably using pulsed-laser detection. This may be achieved by exciting the H atoms with circularly polarized light at 121.6 nm (produced by frequency tripling in a Kr cell) [35], of sufficiently narrow bandwidth to

resolve the $1s(^2S_{1/2}) \rightarrow 2p(^2P_{1/2})$ transition. As shown in figure 3.2, only one of the spin states has a permitted transition for a given circular polarization of probe light; this allows the spin-up and spin-down states to be selectively excited. Ionization from the $2p(^2P_{1/2})$ state may then be achieved using 364.7 nm light. The major

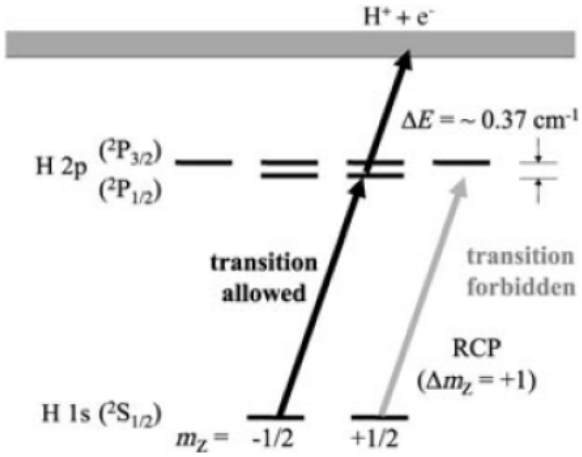

FIGURE 3.2: Resolution of the $2p(^2P_{1/2})$ and $2p(^2P_{3/2})$ states allows the selective ionization of the $m = -1/2$ spin state of ground-state hydrogen using right circularly polarized (RCP) excitation light ($\Delta m = +1$).

disadvantage of this scheme is that the H atoms probed must have a narrow speed distribution, such that the Doppler broadening is less than the $\sim 0.37\ cm^{-1}$ splitting between the $2p(^2P_{1/2})$ and $2p(^2P_{3/2})$ states. This constraint limits the use of this detection method to a few special cases with near monoenergetic speed distributions, such as slow atoms or collimated atomic beams. In contrast to the tiny spin–orbit splitting in the H atom products, the respective spin–obit splitting in the electronic ground state of the Cl atom co-fragments is $\sim 881\ cm^{-1}$ (about 2380 times larger). This means that the Cl atoms may be detected polarization sensitively through a standard (2+1) REMPI (resonance enhanced multiphoton ionization) scheme, using commercial lasers of moderate bandwidth and with no complications arising from Doppler broadening. Figure 3.3 shows the right circularly polarized two-photon excitation of atomic Cl to an intermediate state, followed by an one-photon ionization. Using this scheme, only the $m = -1/2$ state of Cl* and the $m = -3/2$ state of Cl can be detected. When left circularly polarized light is used, the situation is reversed. The polarization, P, of the $Cl(^2P_{1/2})$ atoms is then given by the normalized signal difference between left and right circularly polarized probe light:

$$P = \frac{I(L) - I(R)}{I(L) + I(R)} \tag{3.6}$$

3.2.2 SPH detection with Laser Induced Fluorescence (LIF)

As we saw in the previous section, one of the biggest problems in the detection of the spin polarization in hydrogen atoms was the small hyperfine splitting that destroys selectivity in 1+1 ionization schemes as the one shown in figure 3.2. It is true that spin polarization detection in hydrogen was achieved this way [36] but only for translational temperatures lower than 80K. We can extend this method by photodissociating HBr, for example, at room temperature and at relatively high pressures, and show that the production of SPH is achieved under these conditions, i.e. unlike

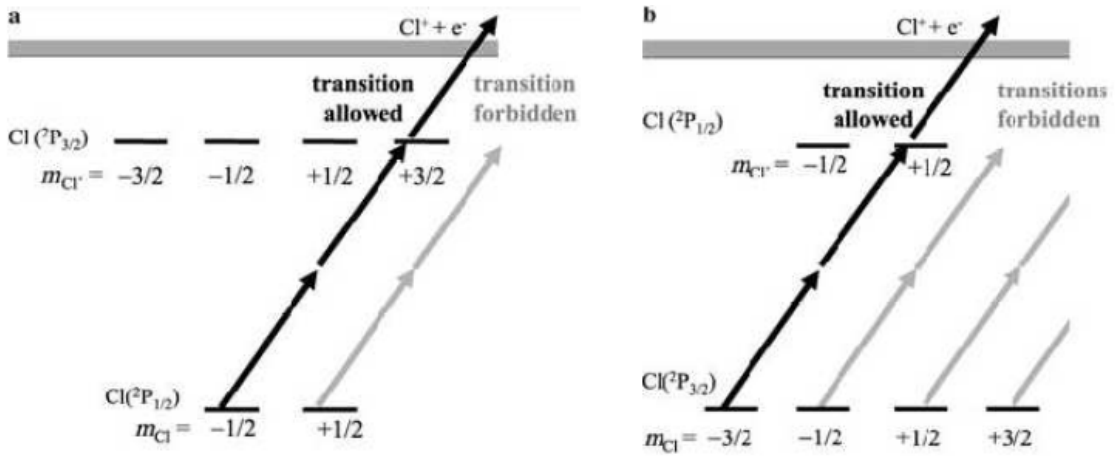

FIGURE 3.3: Two-photon resonant and one-photon ionization transitions for a) $Cl(^2P_{1/2})$ via a $Cl(^2P_{3/2})$ excited state at 236.51 nm, and b) $Cl(^2P_{3/2})$ via a $Cl(^2P_{1/2})$ excited state at 234.62 nm with the light being Right Circularly Polarized (RCP).

many other cases of molecular photodissociation, the photodissociation mechanism of HBr does not change significantly from 15 K to 300K. We can directly detect the SPH spin-selectively on the nanosecond timescale with a new polarization scheme based on fluorescence at 121.6 nm, which does not require hyperfine resolution and hence is independent of the SPH translational temperature, while retaining the excellent detection sensitivity of Lyman-alpha fluorescence. The combination of these two pulsed-laser techniques, and the characterization of the photodissociation of HBr at room temperature, allow us to infer that pulsed densities in excess of 10^{17} cm^{-3} are attainable, and allows the nanosecond-timescale production and detection of SPH.

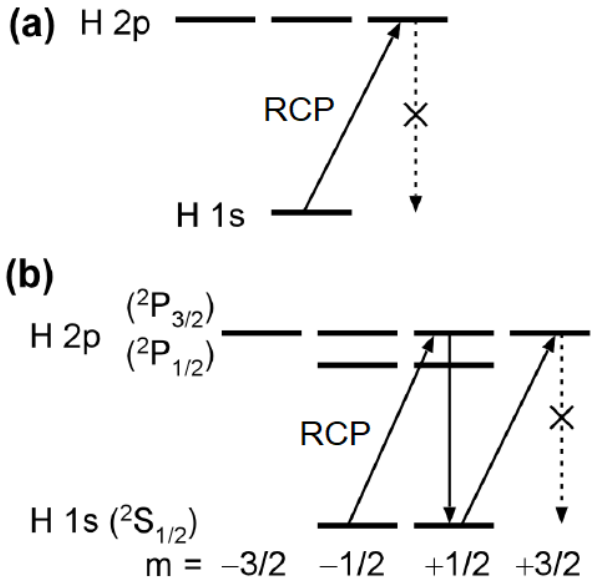

FIGURE 3.4: (a) Energy-level detection scheme, showing that no signal is detected in the limit of no spin-orbit coupling. (b) Similar to (a), but with spin-orbit coupling, showing that only the $m = -1/2$ state is detected using RCP 121.6 nm probe light (see [30]).

The photolysis pulsed laser beam, at 193 nm is circularly polarized and the probe one, at 121.6 nm is circularly polarized as well. After the photodissociation, the H atoms are excited from the 1s $^2S_{1/2}$ to the 2p ^2P_J states using circularly polarized 121.6 nm light. The 121.6 nm fluorescence of excited atoms is detected perpendicular to the propagation of the excitation laser, and a polarizer is used to detect only fluorescence that is linearly polarized along the z-axis, which ensures that the polarization components of the transitions that are observed are those that correspond to $\Delta m = 0$, irrespective of the original polarization of fluorescence (we note that the polarization components of the transitions that corresponded to $\Delta m = \pm 1$ are rejected by the polarizer). It is obvious that this geometry is chosen so that angular momentum selection rules constrain the excitation and fluorescence processes to be allowed for only one of the spin-states, so that the H-atom spin-polarization can be determined along the z-axis. The success of the detection scheme relies on the coupling of the electron's spin to its orbital motion. If the H atoms were to fluoresce very rapidly, on a sub-picosecond timescale where spin-orbit coupling can be ignored, our detector would see no fluorescence since, according to selection rules for linearly polarized fluorescence emission, $\Delta m = 0$ (see figure 3.4(a)). In contrast, for the ~ 1 ns fluorescence lifetime of the 2p state, we see that only atoms that originate from the 1s ($m = -1/2$) "spin-down" state, and that are excited to either of the 2p ^2P_J ($m = +1/2$): no fluorescence can be detected from atoms that originate in the 1s ($m = +1/2$) "spin-up" state (see figure 3.4(b)). The reverse applies for excitation by left circularly polarized light (with $\Delta m = -1$), whereby only the "spin-up" state can be detected. Thus, this detection scheme allows complete spin-state detection selectivity for SPH in the ground state.

3.3 Detection of induced polarization via the macroscopic magnetization

3.3.1 High-density polarized molecular samples produced using an optical centrifuge

In their paper "Ultrafast Magnetization of a Dense Molecular Gas with Optical Centrifuge" [12], A. Milner and cooperators achieved experimentally, on the sub-nanosecond timescale, strong laser-induced magnetization of oxygen gas at room temperature and atmospheric pressure. Their method is based on controlling the electronic spin of paramagnetic molecules by means of manipulating their rotation with an optical centrifuge. In their Letter they demonstrate a technique which is based on the unidirectional rotation of molecules in an optical centrifuge [37, 38]. Unlike optical pumping, it operates far off electronic resonances. Owing to its nonresonant nature, the process can be carried out in a dense gas. Even though only a few percent of O_2 molecules are centrifuged at room temperature, the observed density of polarized electrons exceeds $6 \times 10^{17} cm^{-3}$.

3.3.2 Polarization detection via the macroscopic magnetization

This high degree of gas magnetization is three orders of magnitude above the magnetization typically obtained with optical pumping and can be detectable with a simple pick-up coil. The pick-up coil was centered at the location of the centrifuged volume and it was connected to an oscilloscope, which recorded the time-dependent

electromotive force EMF $\mathcal{E}(t)$. The latter is proportional to the time derivative of the induced magnetization $\vec{M}$ perpendicular to the plane of coil. Using the Faraday's law of induction for the N turns of the coil:

$$\mathcal{E}(t) = -N\frac{\partial \Phi}{\partial t} = -\mu_0 N \frac{\partial (MA)}{\partial t}, \tag{3.7}$$

where Φ is the magnetic flux and A the coil area. Thus, the magnetization was retrieved from the recorded EMF as:

$$M = -\frac{1}{\mu_0 NA}\int_{-\infty}^{t} \mathcal{E}(t')dt', \tag{3.8}$$

where $M = n\mu$, μ is the magnetic moment per molecule and n is the number density of centrifuged molecules. It is $n = \frac{\eta P}{k_B T}$, where P and T are the gas pressure and temperature, k_B is the Boltzmann constant ($k_B = 1.38 \times 10^{-23} J/K$), and η is the fraction of molecules spun by the centrifuge ($\eta = 0.04$, for intensity of laser pulses $\sim 10^{12}\ W/cm^2$, at room temperature). The observed magnetization is shown in figure 3.5. The detected EMF signals are on the scale of 100 μV and correspond to the induced magnetic moment moment of up to 0.16 $\mu_B/molecule$.

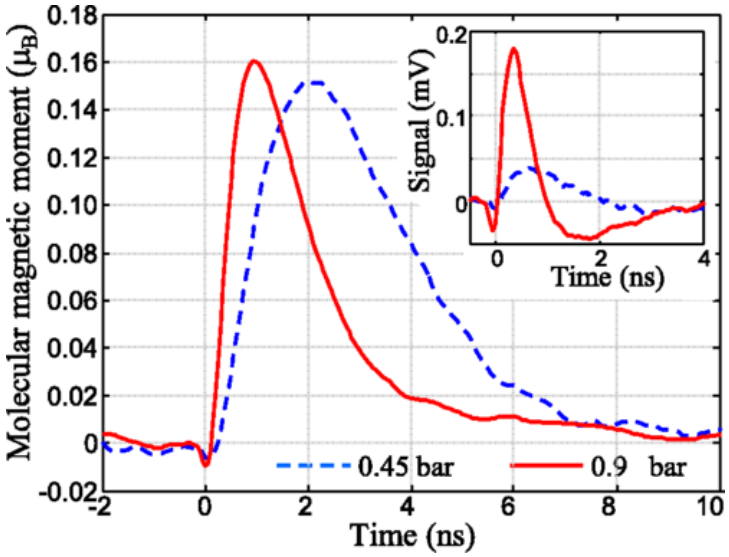

FIGURE 3.5: Centrifuge-induced magnetic moment in oxygen gas, in units of Bohr magneton μ_B. Inset shows raw EMF signals $\mathcal{E}(t)$ recorded under the pressure of 0.45 bar (dashed blue) and 0.9 bar (solid red). Time zero corresponds to the arrival of the centrifuge pulse, whose duration of $\sim 30ps$ was adjusted for the excitation of O_2 molecules to the rotational level $N = 33$ (figure adapted from reference [12]).

3.3.3 Adaptation to the detection of polarized photofragments

We want to adapt the aforementioned method to the detection of polarization induced in the atomic photofragments after molecular dissociation of Cl_2. Below, we give a rough estimation of our signal: The total magnetization $\vec{M}$ is $\vec{M} = \frac{\vec{m}}{V}$, where V is the magnetization volume and $\vec{m}$ is the atomic magnetization:

$$\vec{m}_{atom} = -\frac{g_J \mu_B}{\hbar}\langle \Psi | \vec{J} | \Psi \rangle, \tag{3.9}$$

where $\vec{J}$ is the total angular momentum ($\vec{J} = \vec{L} + \vec{S}$), g_J the Landé g-factor ($g_J = 4/3$, for atomic Cl in the $^2P_{3/2}$ state; see reference [39]) and μ_B is Bohr's magneton ($\mu_B = 9.274 \times 10^{-24}\ J/T$). The component that contributes to the macroscopic magnetization is the parallel component to the z-axis, i.e.

$$m_{atom,z} = -g_J \mu_B M_J, \tag{3.10}$$

where M_J is the projection of $\vec{J}$ along the quantization axis (z-axis).
The interaction of the magnetic field with the pick-up coil (N turns) induces an electromotive force (EMF) across the coil:

$$\mathcal{E}(t) = -N\mu_0 \frac{\partial}{\partial t} \iint \vec{M} \cdot d\vec{S} \tag{3.11}$$

However, the current changes with time, and according to Lenz's law, an induced EMF will arise (rapidly) to oppose that change:

$$\epsilon_L(t) = -\frac{L}{R}\frac{\partial \mathcal{E}}{\partial t}, \tag{3.12}$$

where R is the electrical resistance and L is the inductance, $L = \frac{\mu_0 N^2 A}{l} K$, K is referred as Nagaoka coefficient [40] and depends on the ratio between coil's diameter and length. The other values correspond to permeability of free space ($\mu_0 = 4\pi \times 10^{-7}\ H/m$), the area of cross-section of the coil (A), and the length of coil (l). Eventually, the detected signal will be:

$$V(t) = \mathcal{E}(t) + \epsilon_L(t) = \mathcal{E}(t) - \frac{L}{R}\frac{\partial \mathcal{E}}{\partial t} \tag{3.13}$$

We should notice that $\mathcal{E}(t)$ is proportional to the time derivative of polarized atoms, thus ϵ_L is proportional to the second derivative of that quantity. An important aspect of the method is that the EMF signal reverses every time the orientation of the spins is reversed. This will facilitate the use of a Photoelastic Modulator (PEM) in order to enchance our signal-to-noise ratio (SNR) as described in section 3.4.2.

Suppose that we use a Gaussian pulses with duration (F.W.H.M.-pulse duration) $\tau_p = 6\ ns$, energy $E = 15\ mJ$, wavelength $\lambda = 355\ nm$, beam diameter (spot size) 1.2 mm. The pick-up coil's diameter and length are $d = 2\ mm$ and $l = 3.5\ mm$ respectively, and its distance from the window of the cell is $l_1 = 0.5\ cm$. The coil is relatively short in order to facilitate the acquisition of rapidly changing signal (a measure of this is the value $\tau = L/R \sim 0.36\ ns$). The photodissociation cross section for Cl_2 at 355 nm (room temperature) is $\sigma = 1.7 \times 10^{-19}\ cm^2$/molecule. In order to make some rough estimations for the magnitude of the signal we follow the following steps. The initial available photons are:

$$N_{photons} = \frac{\lambda E}{hc}. \tag{3.14}$$

Applying Beer-Lambert law, the photons that will reach the coil are:

$$N_{photons} e^{-\sigma l_1 n}, \tag{3.15}$$

where n is the particle density and is related to the pressure P(mbar): $n = \frac{P}{1000} 2.44 \times 10^{19}\ cm^{-3}$. Once more, the number of photons that photodissociate Cl_2 in the vicinity

of the coil is:

$$N_{photons} e^{-\sigma l_1 n}(1 - e^{-\sigma l n}) \tag{3.16}$$

Considering that every photon of the previous produces *two* polarized atoms, we can make a rough estimation of the signal for various values of gas pressure, as shown in the following table (3.1):

Pressure (mbar)	Voltage
0.1	4.50 μV
1	45.00 μV
10	0.44 mV
50	1.98 mV
100	3.40 mV
500	5.61 mV

TABLE 3.1: Signal for various values of gas pressure.

However, the expected signal is smaller if we include the following loss factors:

1. Cl atom polarization depends on the angle of the bond with the z-axis (laser circular polarization) as $|cos\theta|$. Angular distribution of Cl photofragments $I(\theta)$: $I(\theta) = I_0(1 + cos^2\theta)$. There is also a factor of $cos\theta$ from the projection of the polarization to the axis parallel to coil axis. Therefore, loss of polarization is given by the ratio of Cl polarization to the total polarization if the photofragments were aligned:

$$\frac{\int_0^\pi cos^2\theta sin\theta(1 + cos^2\theta)d\theta}{\int_0^\pi sin\theta(1 + cos^2\theta)d\theta} = \frac{2}{5}.$$

2. The magnitude of electronic polarization is decreased due to the hyperfine depolarization (by 2)[16]. The loss of polarization from $J = 3/2$ to nuclear spin $I_N = 3/2$ is given by $(k = 1)$:

$$\sum_{F=|J-I_N|}^{|J+I_N|} \frac{(2F+1)^2}{2I_N+1} \begin{Bmatrix} F & F & k \\ J & J & I_N \end{Bmatrix}^2 = \frac{1}{2}.$$

   Due to the fact that our pulses have duration $\tau_p = 6$ ns, it is unattainable to have quantum beating resolution (at nanosecond timescales).

3. Another possible loss factor is the pressure-dependent depolarization [11]. Nevertheless, we cannot predict if the depolarizing collisions affect our signal and how. According to the latter reference, the depolarization due to collisions is negligible for pressures lower than $\sim$ 40 mbar.

4. Finally, the stray capacitance of the coil [41] reduces the efficiency to $\sim$14%, i.e. 7.1 times smaller signal.

Applying the above loss factors to the estimated signal, we get a 35.5 times smaller signal. The reduced values of voltage as a function of pressure are shown in the following table (3.2).

Figure 3.6 shows the time-dependence of the estimated signal for 500 mbar pressure, using a pulse of 6 ns duration.

Pressure (mbar)	Voltage
0.1	0.127 μV
1	1.267 μV
10	12.394 μV
50	55.775 μV
100	95.775 μV
500	158 μV

TABLE 3.2: The reduced signal for various values of gas pressure.

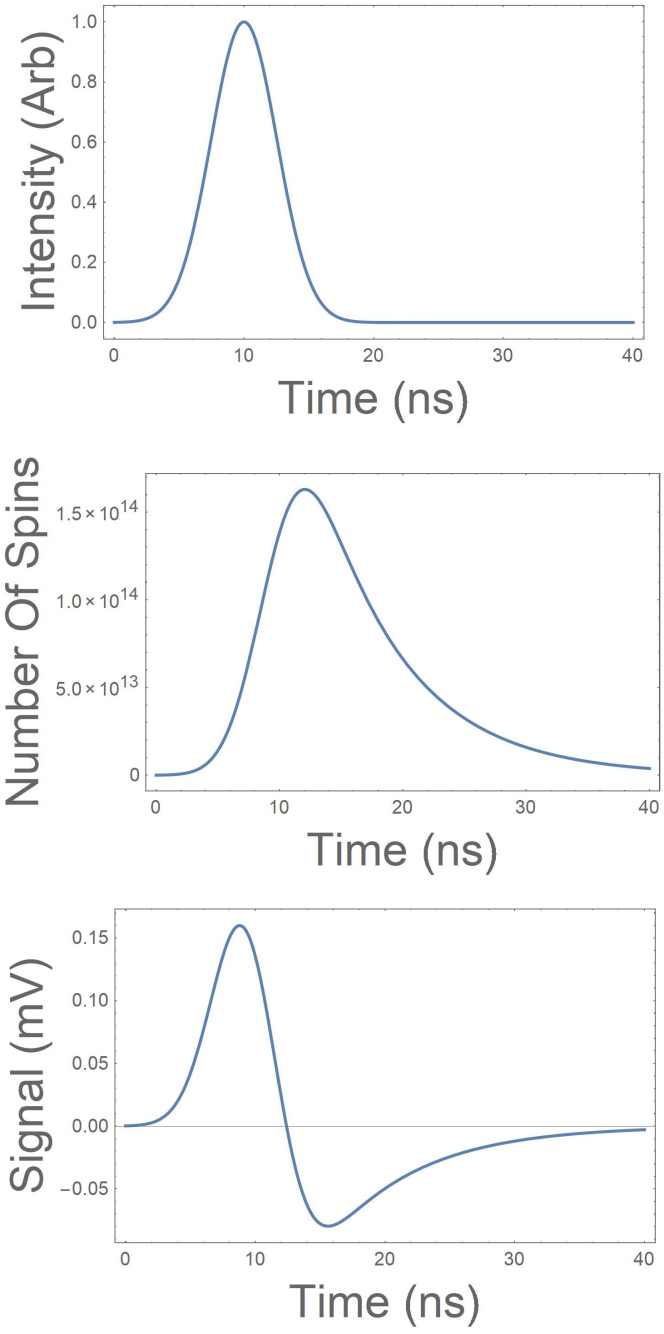

FIGURE 3.6: The first graph shows the Gaussian pulse, which is being used, and the second shows the number of spins which produces the estimated signal (third graph).

Consequently, the expected signal is very small. Various sources produce noise comparable or larger than our signal, so our main goal is to suppress noise and enhance the signal-to-noise ratio (SNR) to at least $\sim$ 10, or greater. Using a photoelastic modulator (PEM) we can double our signal, simply by subtracting the two individual signals for the two polarizations (see paragraph 3.4.2) and also suppress the noise, which should be similar for consecutive pulses.

In the next paragraphs we describe the experimental setup, with emphasis on noise reduction and PEM's integration in our system.

3.4 Methods for noise reduction

As in many experiments, the ability to perform our measurements consists in obtaining a signal that is greater than the noise. The laser we use to dissociate our chlorine molecules is an Nd:Yag system (Quanta-Ray Pro-230) and one of the main sources of noise comes from the laser's Q-switch. We have taken two measures to reduce the noise: a) setting up the experiment far away from the laser, approximately 12 meters away (in an adjust laboratory) and b) integrating into our setup a device called photoelastic modulator (PEM) which allows to invert the polarization of the photolysis laser in a shot-to-shot basis, and thus offering a signal reversal which can lead to an enhancement of the SNR by a factor close to 10. These two measures to enhance the SNR are described in the following paragraphs.

3.4.1 Reducing noise by distance

Our first attempts to realize the experiment was to set it up in close proximity to the dissociation laser, which is an Nd:Yag laser which generates light at 355 nm, and contains a Q-switch synchronized with the arrival of the light. The coil used for the magnetization detection acts like an antenna and picks up this noise with great efficiency. The fact that the electromagnetic noise reduces as $\frac{1}{r}$ (it comes from oscillating electrons, i.e. it is an electric dipole field) dictates that the experiment should be removed as far away from the laser as possible. The Nd:Yag dissociation laser is placed in the "Reaction Dynamics" laboratory on the first floor of the Institute for Electronic Structure and Lasers building. We decided to move the setup to the lab next door ("Ultrafast Laser Micro and Nano Processing Laboratory"), which involved drilling a hole in the wall and transmitting the laser beam in a height of $\sim$ 2.5 meters (close to the sealing) for safety reasons.

This strategy enabled us to reduce the noise by a factor of $\sim$ 10. The fact that this reduction is smaller than what is expected from the ratio $\frac{1}{r}$ indicates that the noise detected in the new location of the experiment is from a new source, different from the laser's Q-switch. This assumption is supported by the fact that the noise has different temporal characteristics, as can be seen in figure 3.7.

3.4.2 Photoelastic Modulator (PEM)

A PEM is an optical device used to modulate the polarization of a light source. Its principle of operation is based on the photoelastic effect, in which a mechanically stressed sample exhibits birefringence proportional to the applied strain. PEMs are resonant devices, each producing oscillating birefringence at a fixed frequency in the low frequency ultrasound range (20 kHz to 100 kHz). In its simplest form the PEM consists of a rectangular bar of a suitable transparent material (fused silica, for example) attached to piezoelectric transducer. The bar vibrates along its long dimension

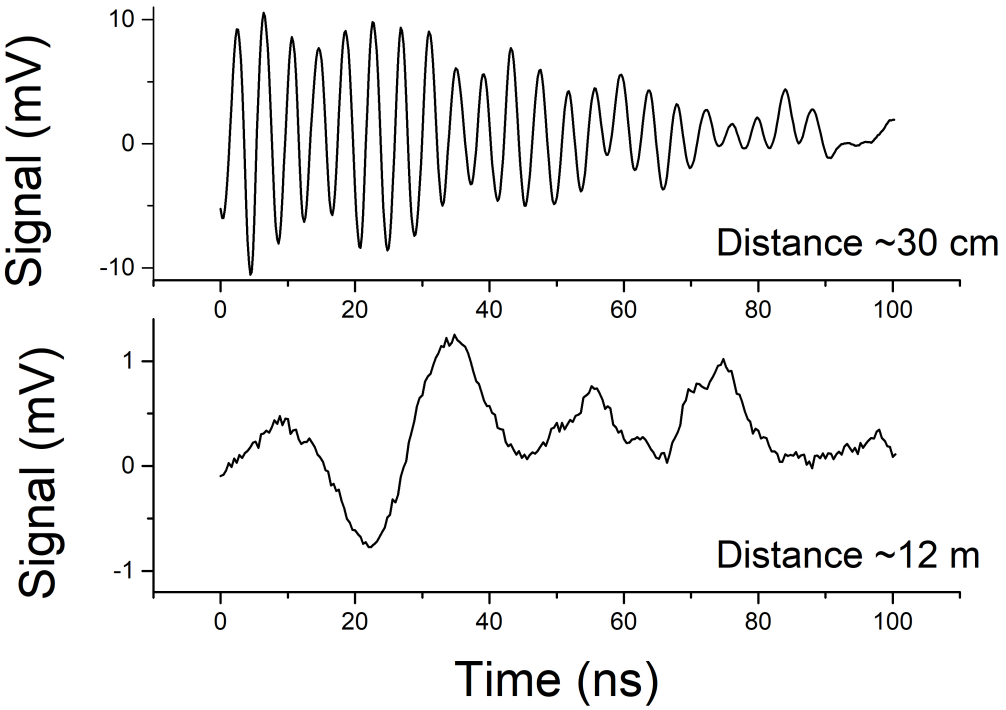

FIGURE 3.7: The noise magnitude at 30 cm and 12 m from Nd:Yag laser.

at a frequency determined by the length of the bar and the speed of a longitudinal sound wave in the optical element material. The transducer is turned to the same frequency and is driven by an electronic circuit which controls the amplitude of vibration. The oscillating birefringence effect is at its maximum at the center of fused silica bar.

If the optical element is compressed the polarization component parallel to the modulator axis travels slightly faster than the vertical component. The horizontal component then "leads" the vertical one after light passes through the modulator. If the optical element is stretched, the horizontal component "lags" behind the vertical one. The phase difference thus created between the two components oscillates as a function of time and is called the retardation or retardance. An important condition for the experiment, occurs when the peak retardation is one-half the wavelength $(\lambda/2)$ of the light. When this happens, the PEM acts as an oscillating half-wave plate. The polarization is modulated between two orthogonal linearly polarized states at twice the PEM's frequency $(2f)$.

Henceforth, we will refer to the PEM's status as high when the optical element of PEM is stretched, and low when it is compressed. Consequently, synchronization to the stress cycle of the PEM allowed the linear polarization of the light to be alternated between vertical and horizontal; after passing though the quarter-wave plate, the photolysis laser polarization alternates between right and left circular polarization states on a shot-to-shot basis.

FIGURE 3.8: PEM (Hinds Instruments)

3.4.3 Synchronization and data acquisition

The most common use of a PEM is in polarimetric measurements with CW laser light. In most of these cases, the goal is to modify the polarization of the CW laser in a harmonic fashion. The PEM provides a signal at the same frequency (and at double the frequency) as the stress cycle and thus of the polarization modulation. This reference signal can be inserted to a lock-in amplifier so that sensitive polarimetric measurements can be performed.

When a PEM is used to modulate the polarization of pulsed lasers (for example ns pulses), such a harmonic modulation cannot be achieved, since the pulse duration is much smaller than the PEM's cycle. The objective in this case is to synchronize the PEM and the arrival of the pulses, in such a way so that for each two consecutive pulses, the polarization is exchanged between two values (for us orthogonal polarizations).

The synchronization of the PEM's stress cycle with the laser beam is attained by using an electronic device called "billbox". This is a frequency divider (which converts the PEM frequency at 100 kHz to 10 Hz), which can insert, on demand, a small delay to synchronize the laser with either a "high" or "low" part of the PEM cycle. When the experiment runs, this delay is inserted every two laser shots (i.e. at 5 Hz). Additionally, the billbox provides with a voltage signal which has a non zero value when the laser is synchronized with a high and zero when the laser is synchronized with a low part of the PEM cycle. The operation of the PEM-billbox system is shown graphically in figure 3.9.

As described in the above sections, PEM changes the light polarization in shot-to-shot basis. Thus, in order to refine our signal, Dr. Sofikitis developed a program in Labview, which allows us to evaluate our measurements in real time. The PC that runs the Labview program is connected to the oscilloscope (LeCroy WaveRunner 44Xi-A), which displays the PEM status (see figure 3.9) and the detected signal. In the Labview interface we have graphs of the signals and their difference. This is feasible, because the program acquires measurements from the two oscilloscope channels (PEM status and signal) and sorts these measurements into two lists. The first list corresponds to the high PEM status and the second to the low one. These lists of measurements and their difference are plotted in real time. We illustrate the respective Labview screen shot in figure 3.10. The program also allows us to average the differences of the signals. In this way, we attain a big noise suppression, as the noise is common in both cases.

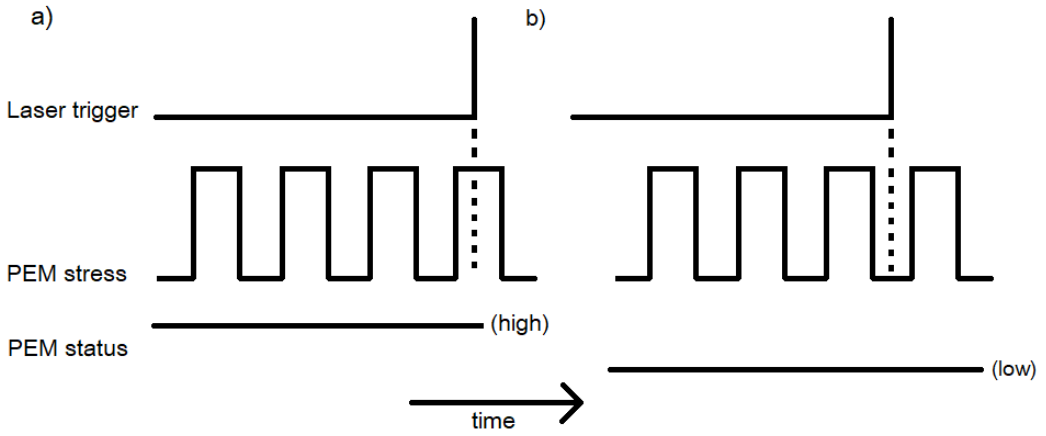

FIGURE 3.9: PEM status (high/low) with respect to the incident laser beam.

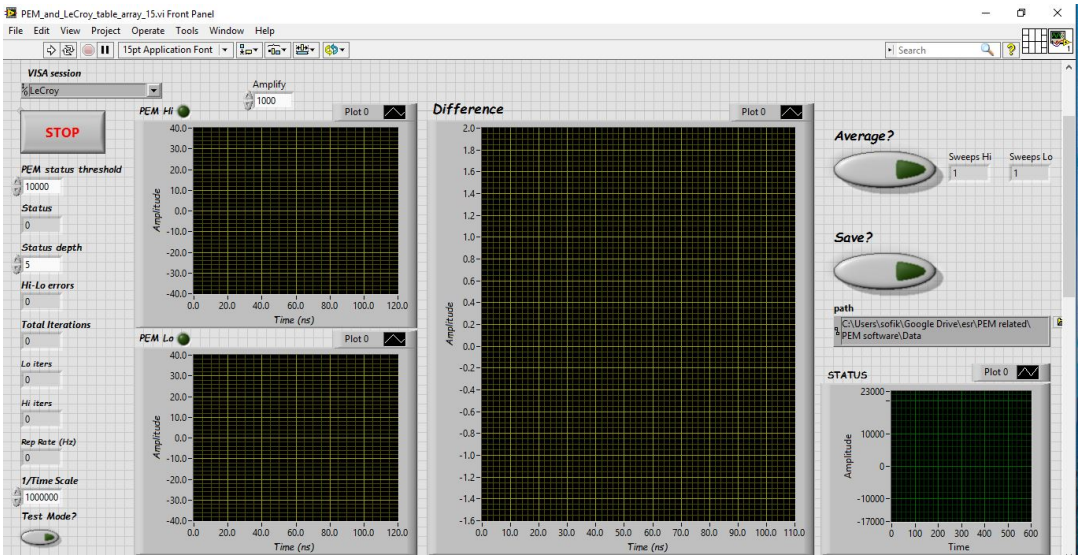

FIGURE 3.10: A screen-shot of Labview program.

3.5 The complete set-up

The main parts of our experimental set-up are: the cell, in which the pick-up coil is centered (figure 3.11). The cell is also connected to the Cl_2 bottle and to the vacuum pump (figure 3.12). We also placed two pressure meters in the cell, one more sensitive to low pressures (0-100 mbar) and the other at pressures between 100-1000 mbar (figure 3.14). Figure 3.15 shows the optical path of the beam. The pulse passes through the mirrors and the first iris in order to reach the PEM, the second iris, the telescope, the tunable wave-plate and finally the cell. The telescope, which consists of a convex and a concave lens, is used for reducing the spot size and the tunable wave-plate to transform the linear polarization to circular.

The experiments for the detection of the macroscopic magnetization produced by the Cl atom polarization are in progress. Currently, the noise levels are below 100 microvolts (for a reasonable number of averaging of the signals), which might already allow detection of spin-polarized samples at a pressure of $\sim$500 mbar. However, we work on noise suppression (<10 μV) by electromagnetically shielding our experiments in order to detect signal for lower pressures, e.g. 40 mbar.

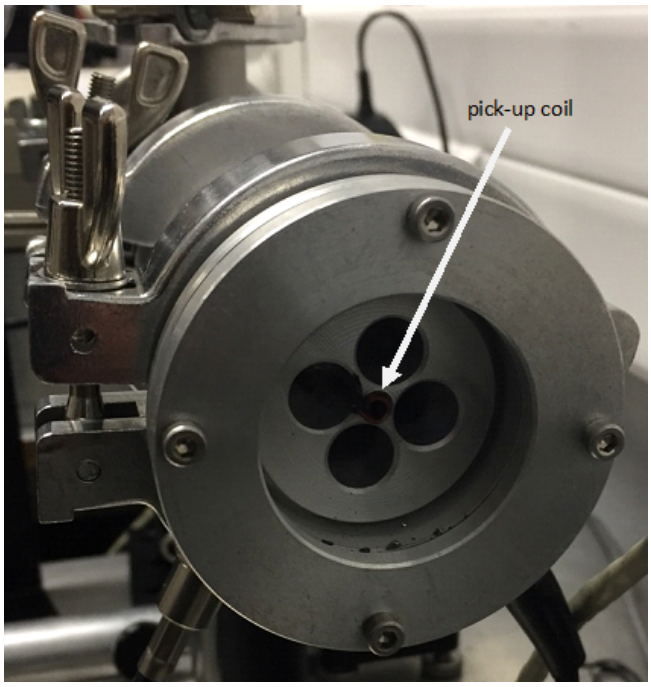

FIGURE 3.11: The front window of the cell. The pick-up coil is centered in the cell, about ~ 0.5 cm from the window.

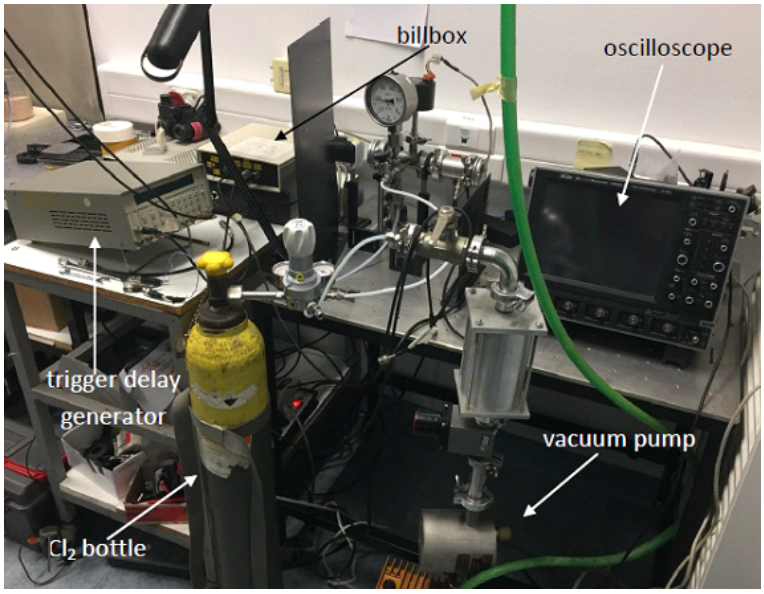

FIGURE 3.12: A part of the experimental set-up.

After this method is successfully implemented for the detection of polarized chlorine atoms, the next step would be to employ it in the detection of high-density polarized deuterium atoms, which are relevant in polarized fusion experiments.

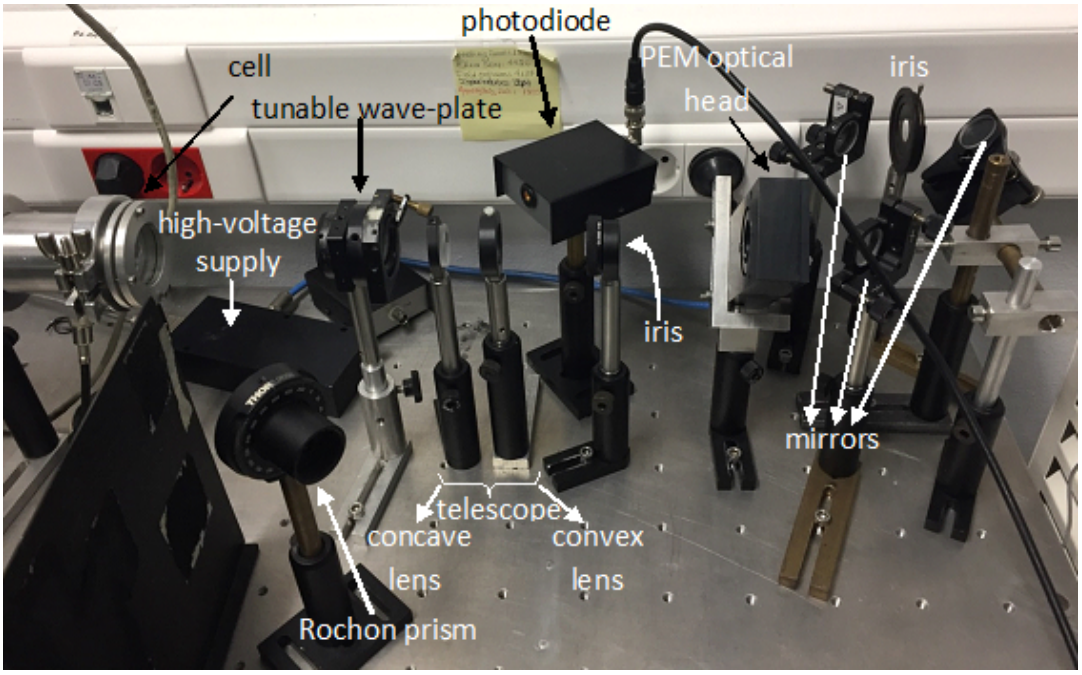

FIGURE 3.13: The optical instrumentation.

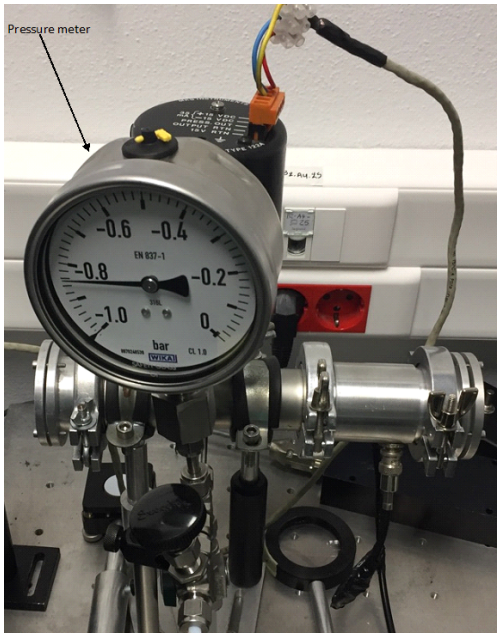

FIGURE 3.14: The second pressure meter, which is used for pressures between 100-1000 mbar.

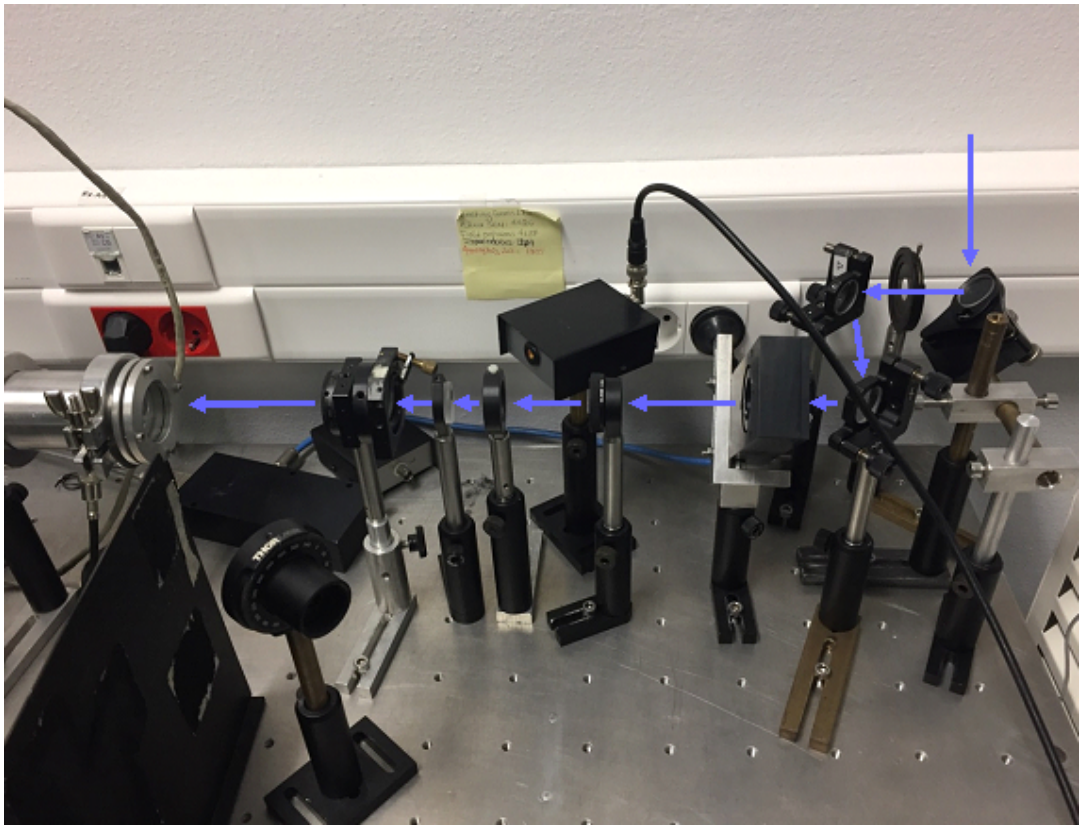

FIGURE 3.15: The optical path of the beam.

Bibliography

[1] S. G. Redsun et al. “Production of highly spin-polarized atomic hydrogen and deuterium by spin-exchange optical pumping”. In: *Phys. Rev. A* 42 (3 1990), pp. 1293–1301. DOI: 10.1103/PhysRevA.42.1293. URL: https://link.aps.org/doi/10.1103/PhysRevA.42.1293.

[2] J. Fisher R. J. Abraham and P. Loftus. *Introduction to NMR Spectroscopy*. Wiley,New York, 1988. ISBN: 978-0-471-91894-3.

[3] Neil A. Gershenfeld and Isaac L. Chuang. “Bulk Spin-Resonance Quantum Computation”. In: *Science* 275.5298 (1997), pp. 350–356. ISSN: 0036-8075. DOI: 10.1126/science.275.5298.350. eprint: http://science.sciencemag.org/content/275/5298/350.full.pdf. URL: http://science.sciencemag.org/content/275/5298/350.

[4] K. Zapfe et al. “High density polarized hydrogen gas target for storage rings”. In: *Review of Scientific Instruments* 66.1 (1995), pp. 28–31. DOI: 10.1063/1.1146388. eprint: http://dx.doi.org/10.1063/1.1146388. URL: http://dx.doi.org/10.1063/1.1146388.

[5] WILLIAM HAPPER. “Optical Pumping”. In: *Rev. Mod. Phys.* 44 (2 1972), pp. 169–249. DOI: 10.1103/RevModPhys.44.169. URL: https://link.aps.org/doi/10.1103/RevModPhys.44.169.

[6] G. Navon et al. “Enhancement of Solution NMR and MRI with Laser-Polarized Xenon”. In: *Science* 271.5257 (1996), pp. 1848–1851. ISSN: 0036-8075. DOI: 10.1126/science.271.5257.1848. eprint: http://science.sciencemag.org/content/271/5257/1848.full.pdf. URL: http://science.sciencemag.org/content/271/5257/1848.

[7] Erhard Steffens and Willy Haeberli. “Polarized gas targets”. In: *Reports on Progress in Physics* 66.11 (2003), p. 1887. URL: http://stacks.iop.org/0034-4885/66/i=11/a=R02.

[8] Alexander B. Barnes et al. “Cryogenic sample exchange NMR probe for magic angle spinning dynamic nuclear polarization”. In: *Journal of Magnetic Resonance* 198.2 (2009), pp. 261 –270. ISSN: 1090-7807. DOI: https://doi.org/10.1016/j.jmr.2009.03.003. URL: http://www.sciencedirect.com/science/article/pii/S1090780709000731.

[9] R. Engels et al. “Polarized fusion”. In: *Physics of Particles and Nuclei* 45.1 (2014), pp. 341–343. ISSN: 1531-8559. DOI: 10.1134/S1063779614010250. URL: https://doi.org/10.1134/S1063779614010250.

[10] C. T. Christou and M. I. Haftel. “Theory of surface recombination of spin-polarized hydrogen”. In: *Few-Body Systems* 7.1 (1989), pp. 1–23. ISSN: 1432-5411. DOI: 10.1007/BF01305258. URL: https://doi.org/10.1007/BF01305258.

[11] Dimitris Sofikitis et al. "Highly Nuclear-Spin-Polarized Deuterium Atoms from the UV Photodissociation of Deuterium Iodide". In: *Phys. Rev. Lett.* 118 (23 2017), p. 233401. DOI: 10.1103/PhysRevLett.118.233401. URL: https://link.aps.org/doi/10.1103/PhysRevLett.118.233401.

[12] A. A. Milner, A. Korobenko, and V. Milner. "Ultrafast Magnetization of a Dense Molecular Gas with an Optical Centrifuge". In: *Phys. Rev. Lett.* 118 (24 2017), p. 243201. DOI: 10.1103/PhysRevLett.118.243201. URL: https://link.aps.org/doi/10.1103/PhysRevLett.118.243201.

[13] A. Airapetian et al. "Measurement of the proton spin structure function g1p with a pure hydrogen target". In: *Physics Letters B* 442.1–4 (1998), pp. 484 – 492. ISSN: 0370-2693. DOI: https://doi.org/10.1016/S0370-2693(98)01341-0. URL: http://www.sciencedirect.com/science/article/pii/S0370269398013410.

[14] T. Wise et al. "Nuclear Polarization of Hydrogen Molecules from Recombination of Polarized Atoms". In: *Phys. Rev. Lett.* 87 (4 2001), p. 042701. DOI: 10.1103/PhysRevLett.87.042701. URL: https://link.aps.org/doi/10.1103/PhysRevLett.87.042701.

[15] Robert Altkorn, Richard N. Zare, and Chris H. Greene. "Depolarization of optically prepared molecules by two randomly oriented spins". In: *Molecular Physics* 55.1 (1985), pp. 1–9. DOI: 10.1080/00268978500101121. eprint: http://dx.doi.org/10.1080/00268978500101121. URL: http://dx.doi.org/10.1080/00268978500101121.

[16] T. Peter Rakitzis. "Highly Spin-Polarized Atoms and Molecules from Rotationally State-Selected Molecules". In: *Phys. Rev. Lett.* 94 (8 2005), p. 083005. DOI: 10.1103/PhysRevLett.94.083005. URL: https://link.aps.org/doi/10.1103/PhysRevLett.94.083005.

[17] Luis Rubio-Lago et al. "Time-dependent polarization transfer from molecular rotation to nuclear spin". In: *Phys. Rev. A* 74 (4 2006), p. 042503. DOI: 10.1103/PhysRevA.74.042503. URL: https://link.aps.org/doi/10.1103/PhysRevA.74.042503.

[18] Nate C.-M. Bartlett et al. "Time-dependent depolarization of aligned HD molecules". In: *Phys. Chem. Chem. Phys.* 11 (1 2009), pp. 142–147. DOI: 10.1039/B814133A. URL: http://dx.doi.org/10.1039/B814133A.

[19] Christopher J. Foot. *Atomic Physics*. Oxford Master Series in Atomic, Optical and Laser Physics. Oxford University Press Inc., 2005. ISBN: 0 19 850695 3.

[20] Norman F. Ramsey. "Theory of Molecular Hydrogen and Deuterium in Magnetic Fields". In: *Phys. Rev.* 85 (1 1952), pp. 60–65. DOI: 10.1103/PhysRev.85.60. URL: https://link.aps.org/doi/10.1103/PhysRev.85.60.

[21] H. G. Kolsky et al. "Nuclear Radiofrequency Spectra of H_2 and D_2 in High and Low Magnetic Fields". In: *Phys. Rev.* 87 (3 1952), pp. 395–403. DOI: 10.1103/PhysRev.87.395. URL: https://link.aps.org/doi/10.1103/PhysRev.87.395.

[22] G. F. Newell. "Magnetic Shielding Constant of H_2". In: *Phys. Rev.* 80 (3 1950), pp. 476–477. DOI: 10.1103/PhysRev.80.476. URL: https://link.aps.org/doi/10.1103/PhysRev.80.476.

[23] J. M. B. Kellogg et al. “The Magnetic Moments of the Proton and the Deuteron. The Radiofrequency Spectrum of H_2 in Various Magnetic Fields”. In: *Phys. Rev.* 56 (8 1939), pp. 728–743. DOI: 10.1103/PhysRev.56.728. URL: https://link.aps.org/doi/10.1103/PhysRev.56.728.

[24] Michael I. Rosen. “Niels Hendrik Abel and Equations of the Fifth Degree”. In: *The American Mathematical Monthly* 102.6 (1995), pp. 495–505. ISSN: 00029890, 19300972. URL: http://www.jstor.org/stable/2974763.

[25] A J Orr-Ewing, and R N Zare. “Orientation and Alignment of Reaction Products”. In: *Annual Review of Physical Chemistry* 45.1 (1994), pp. 315–366. DOI: 10.1146/annurev.pc.45.100194.001531. eprint: https://doi.org/10.1146/annurev.pc.45.100194.001531. URL: https://doi.org/10.1146/annurev.pc.45.100194.001531.

[26] Norman F. Ramsey and Henry R. Lewis. “Theory of Hydrogen Deuteride in Magnetic Fields”. In: *Phys. Rev.* 108 (5 1957), pp. 1246–1250. DOI: 10.1103/PhysRev.108.1246. URL: https://link.aps.org/doi/10.1103/PhysRev.108.1246.

[27] W. E. Quinn et al. “Radio-Frequency Spectra of Hydrogen Deuteride in Strong Magnetic Fields”. In: *Phys. Rev.* 112 (6 1958), pp. 1929–1940. DOI: 10.1103/PhysRev.112.1929. URL: https://link.aps.org/doi/10.1103/PhysRev.112.1929.

[28] J. M. B. Kellogg et al. “An Electrical Quadrupole Moment of the Deuteron The Radiofrequency Spectra of HD and D_2 Molecules in a Magnetic Field”. In: *Phys. Rev.* 57 (8 1940), pp. 677–695. DOI: 10.1103/PhysRev.57.677. URL: https://link.aps.org/doi/10.1103/PhysRev.57.677.

[29] T. Peter Rakitzis and Theofanis N. Kitsopoulos. “Measurement of Cl and Br photofragment alignment using slice imaging”. In: *The Journal of Chemical Physics* 116.21 (2002), pp. 9228–9231. DOI: 10.1063/1.1473801. eprint: http://dx.doi.org/10.1063/1.1473801. URL: http://dx.doi.org/10.1063/1.1473801.

[30] Dimitris Sofikitis et al. “Laser detection of spin-polarized hydrogen from HCl and HBr photodissociation: Comparison of H- and halogen-atom polarizations”. In: *The Journal of Chemical Physics* 129.14 (2008), p. 144302. DOI: 10.1063/1.2989803. eprint: http://dx.doi.org/10.1063/1.2989803. URL: http://dx.doi.org/10.1063/1.2989803.

[31] Dimitrios Sofikitis et al. “Highly spin-polarized deuterium atoms from the UV dissociation of Deuterium Iodide”. In: 118 (Oct. 2016).

[32] R. J. Van Brunt and R. N. Zare. “Polarization of Atomic Fluorescence Excited by Molecular Dissociation”. In: *The Journal of Chemical Physics* 48.9 (1968), pp. 4304–4308. DOI: 10.1063/1.1669773. eprint: http://dx.doi.org/10.1063/1.1669773. URL: http://dx.doi.org/10.1063/1.1669773.

[33] T. P. Rakitzis et al. “Spin-Polarized Hydrogen Atoms from Molecular Photodissociation”. In: *Science* 300.5627 (2003), pp. 1936–1938. ISSN: 0036-8075. DOI: 10.1126/science.1084809. eprint: http://science.sciencemag.org/content/300/5627/1936.full.pdf. URL: http://science.sciencemag.org/content/300/5627/1936.

[34] Laurens D. A. Siebbeles et al. "Vector properties in photodissociation: Quantum treatment of the correlation between the spatial anisotropy and the angular momentum polarization of the fragments". In: *The Journal of Chemical Physics* 100.5 (1994), pp. 3610–3623. DOI: 10.1063/1.466402. eprint: http://dx.doi.org/10.1063/1.466402. URL: http://dx.doi.org/10.1063/1.466402.

[35] G. G. Balint-Kurti et al. "Vector correlations and alignment parameters in the photodissociation of HF and DF". In: *The Journal of Chemical Physics* 116.24 (2002), pp. 10760–10771. DOI: 10.1063/1.1476937. eprint: http://dx.doi.org/10.1063/1.1476937. URL: http://dx.doi.org/10.1063/1.1476937.

[36] H. Rottke and H. Zacharias. "Generation of nuclear-spin-polarized protons by resonant ionization of hydrogen atoms". In: *Phys. Rev. A* 33 (1 1986), pp. 736–738. DOI: 10.1103/PhysRevA.33.736. URL: https://link.aps.org/doi/10.1103/PhysRevA.33.736.

[37] Joanna Karczmarek et al. "Optical Centrifuge for Molecules". In: *Phys. Rev. Lett.* 82 (17 1999), pp. 3420–3423. DOI: 10.1103/PhysRevLett.82.3420. URL: https://link.aps.org/doi/10.1103/PhysRevLett.82.3420.

[38] D. M. Villeneuve et al. "Forced Molecular Rotation in an Optical Centrifuge". In: *Phys. Rev. Lett.* 85 (3 2000), pp. 542–545. DOI: 10.1103/PhysRevLett.85.542. URL: https://link.aps.org/doi/10.1103/PhysRevLett.85.542.

[39] Leon J. Radziemski and Victor Kaufman. "Wavelengths, Energy Levels, and Analysis of Neutral Atomic Chlorine (Cl i)". In: *J. Opt. Soc. Am.* 59.4 (1969), pp. 424–443. DOI: 10.1364/JOSA.59.000424. URL: http://www.osapublishing.org/abstract.cfm?URI=josa-59-4-424.

[40] Nagaoka H. "The Inductance Coefficients of Solenoids". In: *The Journal of the College of Science, Imperial University of Tokyo, Japan* 27.6 (1909), pp. 1–33. URL: http://jairo.nii.ac.jp/0021/00019828/en.

[41] A. Massarini U. Reggiani G. Grandi M.K. Kazimierczuk. "Stray capacitances of single-layer air-core inductors for high-frequency applications". In: *IEEE Xplore Digital Library* (2002), pp. 1384–1388. DOI: 10.1109/IAS.1996.559246. URL: http://ieeexplore.ieee.org/document/559246.